OCEAN APPLICATIONS TECHNICAL NOTE 17

Vortex stretching and bottom torques in the Bryan - Cox Ocean Circulation Model

by

M. J. Bell

Met Office
FitzRoy Road, Exeter, Devon. EX1 3PB

1. Introduction

Ocean models have been used for many years in integrations of 10-100 years in length to study the role of the oceans in the Earth's climate. More recently a number of groups have assimilated observations into ocean models to produce ocean analyses or forecasts (Ji et al. 1995). Much effort has concentrated on the tropical Pacific ocean. This has focused attention on the rapid development of thermal biases, particularly in the equatorial east Pacific, in ocean models driven by the available wind stress fields (Anderson et al. 1997 section 4). The Forecasting Ocean Atmosphere Model (FOAM) group at the Met. Office have developed a global assimilation system which will be operational from September 1997. The main focus of this group is the North Atlantic. Rapidly developing errors in the thermal field in this region again affect the quality of the ocean analyses.

The difference at 100 m depth between the monthly mean potential temperature field from the third month of integration of a FOAM integration and the Levitus (1982) climatology in the North Atlantic is displayed in figure 1. The model was started on 15 February from a state of rest with the Levitus (1982) potential temperature and salinity fields for February. Figure 1 displays the difference between fields valid for May. No data were assimilated in the integrations displayed in this paper. The details of the FOAM model are described in appendix A.

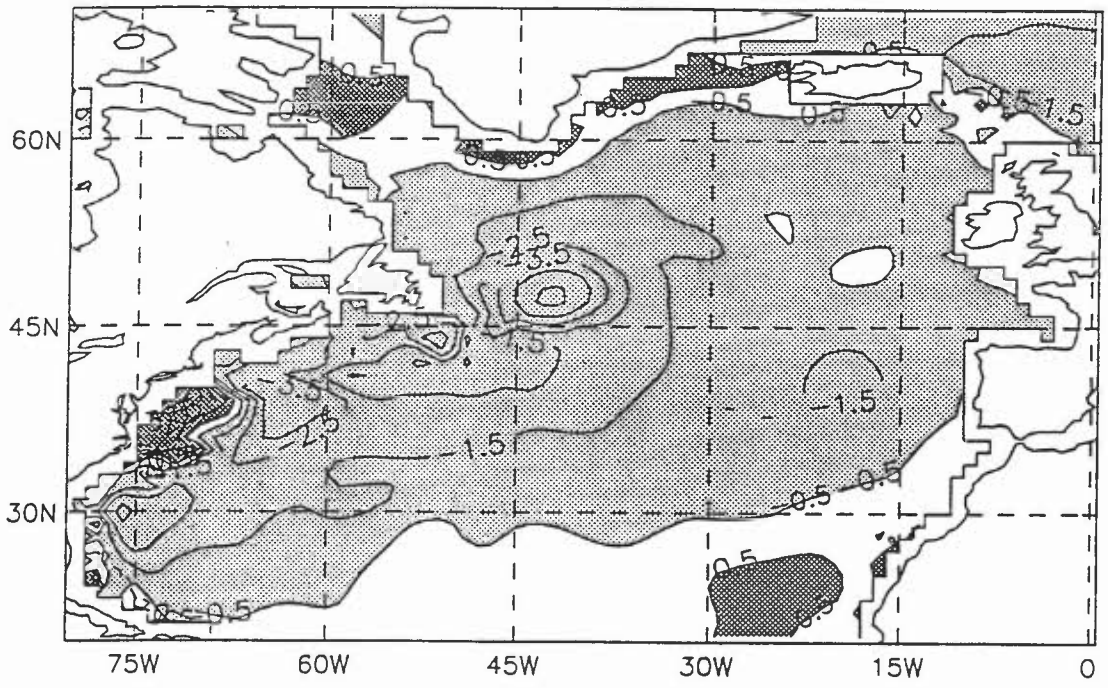

Figure 1: Monthly mean potential temperature at 100 m depth from third month (May) of integration of FOAM model minus Levitus (1982) climatology. The contour interval is 1 K. Values less (greater) than -0.5 (+0.5) K are shaded lightly (darkly).

The most notable features in figure 1 are the "cold pool" to the east of the Flemish Cap and the warm pool just to the north of Cape Hatteras. The cold pool reaches to about 300 m depth and has a central value of -4 K. It varies somewhat with season but seems to be quite robust in the integrations performed at the Met. Office at 1° or 1.25° resolution. It also seems to be apparent in the robust diagnostic integrations of Sarmiento & Bryan (1982 figure 6b) and the 10 year assimilation of Rosati et al (1995 figure 9a). In longer integrations without any data assimilation the cold pool changes shape extending further to the east; after one year of integration it extends from 45 to 30 °W. The warm pool reaches to about 600 m depth and reflects the notorious failure of the Gulf Stream in Bryan-Cox ocean models of this resolution to separate from the coast at Cape Hatteras.

The barotropic streamfunction for the third month of the same integration is illustrated in figure 2a. It is notable that the maximum eastward transport by the Gulf Stream at 55 °W is only 25 Sv and that the recirculations to the north and south of the Gulf Stream at this longitude are absent and very weak respectively. There is strong observational evidence for a northern recirculation gyre (Hogg et al 1986, Richardson 1985) and Richardson (1985) estimates that the mean barotropic circulation by the Gulf Stream at 55 °W is about 90 Sv. Although there are seasonal variations in the strength of the sub-tropical gyre and Richardson's calculation is not exactly comparable with the model's it seems clear that there is a major discrepancy.

The diagnostic calculation of the barotropic flow by Greatbatch et al. (1991 hereafter GFGL) produces a streamfunction which contains strong recirculation gyres both north and south of the Gulf Stream. Their streamfunction, which is reproduced in figure 2b, also has a strong north-eastward flow to the east of the Flemish Cap and a southward flow to its west. Their calculation was performed on a 1° grid using essentially the same density and wind stress fields as employed by the FOAM model but unsmoothed topography. GFGL infer (their figure 6) that the recirculations and flows around the Flemish Cap in their model are largely "forced" by the bottom pressure torque. The calculations of Myers et al. (1996) using a higher resolution model support the findings of GFGL.

Diagnostics of the heat transports to the east of the Flemish Cap in the FOAM model show that southward advection of cold water from the north by the wind-driven Ekman flux produces cooling which can account for the development of the "cold pool". Although the strength of this advection is subject to some uncertainty it does not appear likely that inaccuracy of the wind stress can account for the development of the "cold pool". The magnitude and shape of the "cold pool" could, however, be accounted for by advection across the strong thermal gradient in this region by the barotropic current calculated by GFGL (see appendix B for more details).

Many investigators have studied the separation from the coast of the Gulf Stream or the Kuroshio current using models with various formulations, resolutions and boundary conditions (e.g. Hurlburt et al. 1996). Dengg et al. (1996), who provide a review of Gulf Stream separation, emphasize the point that the performance of these models should sharpen our understanding of

Figure 2a

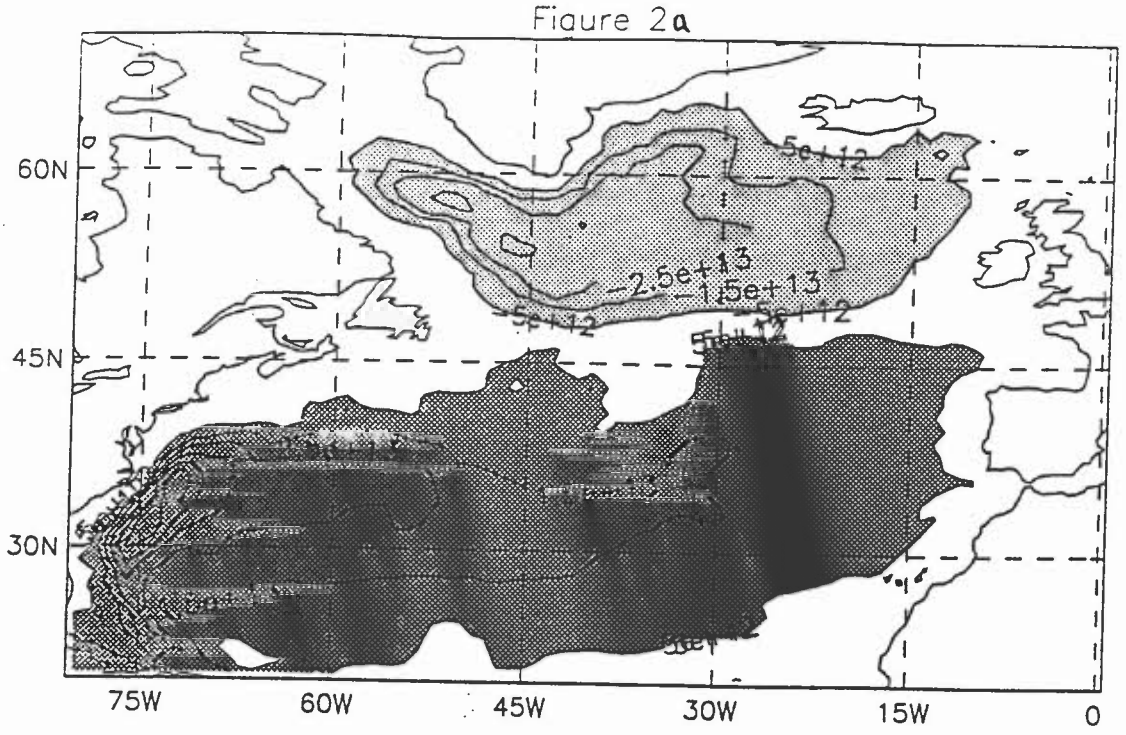

Figure 2b

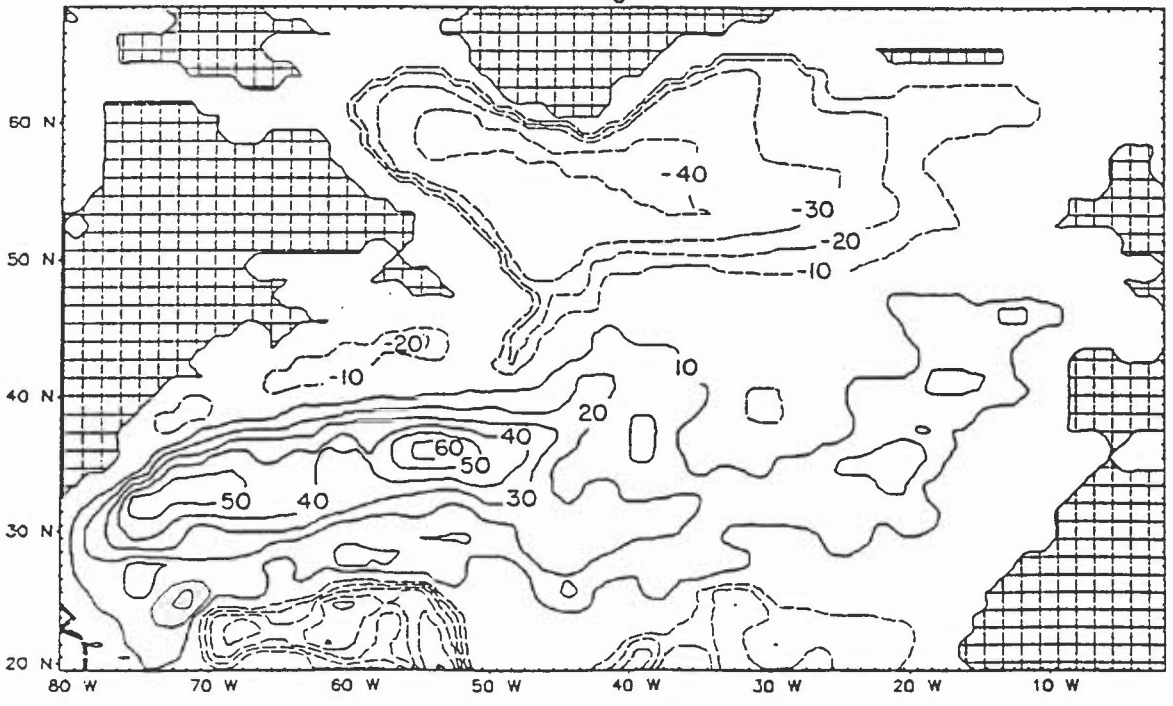

Figure 2: (a) Monthly mean barotropic streamfunction from third month of integration of FOAM model. (b) The barotropic streamfunction obtained by the diagnostic calculation of Greatbatch et al. (1991). The contour interval is 10 Sv (=10^{13} cm^3 s^{-1}) in both cases.

Gulf Stream separation and enable assessment of the many theories of Gulf Stream separation. Although Chao et al. (1997) have reported some success in obtaining Gulf Stream separation in a Cox type model, the results of Beckmann et al. (1994) demonstrate that even Cox models of $1/6^0$ resolution can have a poor representation of Gulf Stream separation. Also although most models fail to represent Gulf Stream separation at 1^0 resolution this is the resolution of the topography used by Myers et al. (1996). They also use a momentum diffusion coefficient of 10^4 m^2 s^{-1} which is slightly larger than that used by the FOAM model. Thus it seems that the barotropic flow is quite sensitive to the model formulation and that some models might have significantly superior representations of it than others at moderate resolutions. This would be particularly important for climate simulations as long integrations are not affordable at high resolution.

The Bryan-Cox model uses a stepped topography and has the important property that the vertical velocity at the bottom of the model on the tracer grid is zero. Since the vortex stretching of a full column of water is determined by the vertical velocity at the bottom of the ocean and is closely related to the bottom pressure torque it is of interest to enquire how bottom pressure torques are represented in the Bryan-Cox model. This is the main purpose of this paper.

Vertically averaged vorticity diagnostics can be formed in three ways (Mertz & Wright 1992):

(1) the curl can be taken of terms in the vertical average of the momentum equations

(2) the curl can be taken of the vertical integral of the momentum equations

(3) the vertical integral can be taken of the curl of the momentum equations.

(The depth average of the curl of the momentum equation is directly related to the third set of diagnostics so need not be considered.) As described in more detail in sections 2 and 4, there are important differences between the terms arising in these formulations. The interaction with the bottom topography is related to JEBAR (joint effect of baroclinicity and relief) in the first set of diagnostics, the bottom pressure torque in the second set, and the vortex stretching in the third set. Ezer & Mellor (1994) have calculated the second set of diagnostics for their sigma coordinate model and Wells & de Cuevas (1995) investigated area averages of the second set of diagnostics for the Antarctic Circumpolar Current in the FRAM version of the Cox model. GFGL and other papers on diagnostic models must calculate the first set of diagnostics and usually also calculate some terms for the second set of diagnostics. Section 3 presents calculations of the first and second set of diagnostics for the FOAM model and section 4 discusses the third set of diagnostics.

Attention is concentrated on diagnostics for integrations of only 3 months duration for several reasons in addition to those already mentioned. Firstly the barotropic flow adjusts to a given density field within about a month of integration. For a realistic density field a model suitable for climate simulations should produce a realistic barotropic flow which does not result in rapidly developing density errors. The subsequent maintenance of the correct density field is, of course,

likely to involve the correct representation of many other processes (e.g. Ezer & Mellor 1992). It is best to isolate problems involving fewer processes and shorter timescales from those which develop more slowly. Finally as there are many theories of Gulf Stream separation, there are many factors on which it is thought the separation may depend. In this situation relevant diagnostics of the flow are of particular value.

Section 2 of this paper describes the formulation of the first two sets of vorticity diagnostics more fully and relates them to the diagnostic calculations of GFGL and the literature on JEBAR and bottom pressure torques. Section 3 illustrates the contributions to these two sets of vertically averaged vorticity tendencies in the FOAM model and establishes which contributions are dominant. Guided by the results of section 3, section 4 discusses the main terms in the third form of vertically averaged vorticity tendency next to a topographic step in the Cox model and relates the vortex stretching near the bottom of the model to the bottom pressure torque. The streamfunctions "driven" by various contributions to the total torque are diagnosed and discussed in section 5. The concluding section summarises the main results and discusses opportunities for further work.

2. Definition of the first two sets of vorticity diagnostics

The latitudinal and longitudinal components of the primitive equation form of the momentum equations on the sphere may be written as

$$\begin{aligned} \partial u/\partial t &= -\{(\underline{u}.\underline{\nabla})u - \frac{uv\tan\phi}{a}\} + fv - \frac{\partial p/\partial\lambda}{\rho_0 a\cos\phi} + \rho_0^{-1}\partial\tau_\lambda/\partial z + F_\lambda \\ \partial v/\partial t &= -\{(\underline{u}.\underline{\nabla})v + \frac{u^2\tan\phi}{a}\} - fu - \frac{\partial p/\partial\phi}{\rho_0 a} + \rho_0^{-1}\partial\tau_\phi/\partial z + F_\phi \quad . \end{aligned} \tag{1}$$

Here, λ is longitude, ϕ is latitude, u the eastward and v the northward velocity components, a the Earth's radius, $\underline{u}$ the full three dimensional velocity vector, $\underline{\nabla}$ the vector gradient, f is the Coriolis parameter and p the pressure. The vertical derivatives of the stresses τ_λ and τ_ϕ denote the vertical diffusive fluxes of momentum and F_λ and F_ϕ denote the horizontal diffusive fluxes. per unit volume. In the Bryan-Cox model the latter terms are the components of $\nu\nabla^2\underline{u}$. The five terms on the right hand side of (1) represent respectively the non-linear advection (of momentum), the Coriolis acceleration, the pressure gradient force (per unit mass) and the vertical and horizontal diffusion of momentum.

The first two sets of vorticity diagnostics are obtained by taking vertical integrals or averages of each of the terms of (1) over the depth, H, of the fluid and then taking the curl

$$curl(a_\lambda, a_\phi) = \frac{1}{a\cos\phi}\{\partial a_\phi/\partial\lambda - \partial(a_\lambda\cos\phi)/\partial\phi\} \quad . \tag{2}$$

The first set is obtained by taking the curl of the vertical average of the components:

$$vertical\ average(a) = \frac{1}{H}\int_{-H}^{0} a\ dz\ . \qquad (3)$$

The second set is obtained by taking the curl of the vertical integral of the components:

$$vertical\ integral(a) = \int_{-H}^{0} a\ dz\ . \qquad (4)$$

This approach and the inter-relationship between the two sets of diagnostics is discussed by Mertz & Wright (1992).

Two of the five terms, namely those arising from the non-linear advection and horizontal diffusive flux of momentum, have no special names for either set of diagnostics and will be referred to as the advection term and viscous torque respectively. The term arising from the vertical diffusion includes and, in the absence of bottom drag as in the FOAM model, only depends on the input of wind stress at the surface of the ocean. This term will be referred to as the curl of the wind stress for both sets of diagnostics though this name is only strictly accurate for the second set of diagnostics.

Interpretation of Pressure terms

The pressure in ocean models is often written as the sum of the surface pressure, p_s, and the integral of the hydrostatic pressure gradient

$$p(z,\lambda,\phi) = p_s(\lambda,\phi) + \int_{z}^{0} \rho g\ dz\ ; \qquad (5)$$

The first set of vorticity diagnostics are designed so that when (5) is substituted into (1) and the vertical average and then the curl is taken, there is no net contribution from the surface pressure term. This is simply because the vertical average of p_s is p_s and curl (grad p_s) = 0. Thus the pressure gradient term for the first set of vorticity diagnostics depends only on the ocean's density structure and the bottom topography. This term, referred to as JEBAR (joint effect of baroclinicity and relief), was first studied by Holland & Hirschman (1972) and Sarkisyan & Ivanov (1971). Mertz & Wright (1992 equation (12)) show that "JEBAR represents precisely the geostrophic correction to the topographic stretching to account for the fact that the bottom average velocity, not the depth-average velocity, yields topographic vortex-tube stretching".

For the second set of vorticity diagnostics the decomposition (5) is not used but since curl (grad p) is zero only the pressure gradients at the ocean bottom, p_b, contribute. Using (1) and (2):

$$curl \int_{-H}^{0} \frac{1}{a} \left(- \frac{\partial p/\partial \lambda}{\cos\phi}, - \partial p/\partial \phi \right) dz$$

$$= \frac{1}{a^2 \cos\phi} \{ \partial H/\partial \lambda \; \partial p_b/\partial \phi - \partial H/\partial \phi \; \partial p_b/\partial \lambda \} \qquad (6)$$

$$= \underline{\nabla} H \wedge \underline{\nabla} p_b = J(H, p_b) \; .$$

So the pressure term in the second set of vorticity diagnostics is the bottom pressure torque.

Interpretation of Coriolis terms

The standard version of the Bryan-Cox code and the diagnostic model of GFGL exclude external gravity waves by imposing a rigid lid condition on the ocean surface. With this condition the vertically integrated flow (U, V) is non-divergent and can be represented by a streamfunction ψ:

$$U \equiv \int_{-H}^{0} u \; dz = -\frac{1}{a} \partial\psi/\partial\phi \; ; \; V \equiv \int_{-H}^{0} v \; dz = \frac{1}{a\cos\phi} \partial\psi/\partial\lambda \; . \qquad (7)$$

The contribution from the Coriolis terms to the first set of vorticity diagnostics can then be written using (1) and (7) as:

$$\frac{1}{a} curl \{ \frac{f}{H} \left(\frac{1}{\cos\phi} \partial\psi/\partial\lambda, \; \partial\psi/\partial\phi \right) \} = J(f/H, \; \psi) \; . \qquad (8)$$

So for the first set of vorticity diagnostics the Coriolis term represents the vertical mean transport across f/H contours.

The contribution from the Coriolis terms to the second set of vorticity diagnostics is:

$$\frac{1}{a} curl \{ f \left(\frac{1}{\cos\phi} \partial\psi/\partial\lambda, \; \partial\psi/\partial\phi \right) \} = - \beta \frac{\partial\psi/\partial\lambda}{a\cos\phi} = -\beta V \; . \qquad (9)$$

βV is often referred to as the Sverdrup transport.

The diagnostic model of GFGL calculates ψ from the first set of diagnostics by assuming that the flow is driven by the wind stress forcing and interaction with the bottom topography (as represented by JEBAR) and that the non-linear and "viscous torque" terms are negligible. After specifying boundary conditions on ψ at the eastern boundary, ψ can be integrated around f/H contours (see (8)) the flow across f/H contours being forced by the wind stress curl and JEBAR. Mellor et al. (1982) pioneered this approach with more robust formulations than (8) for the integration of ψ.

Figure 3a

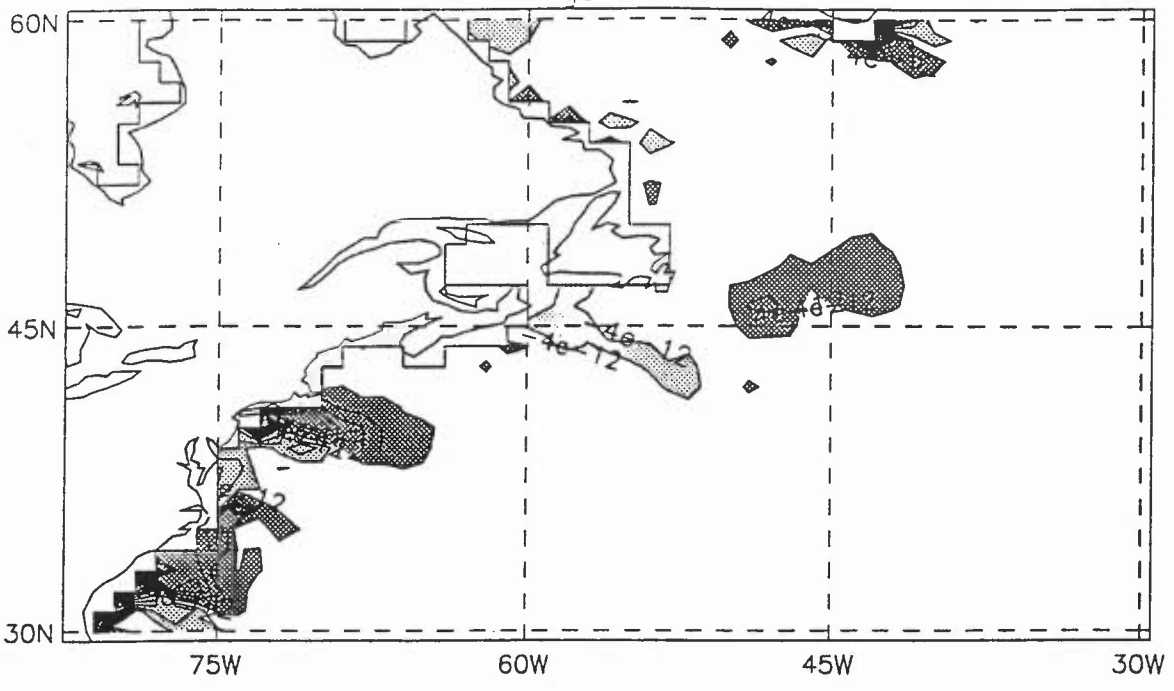

Figure 3b

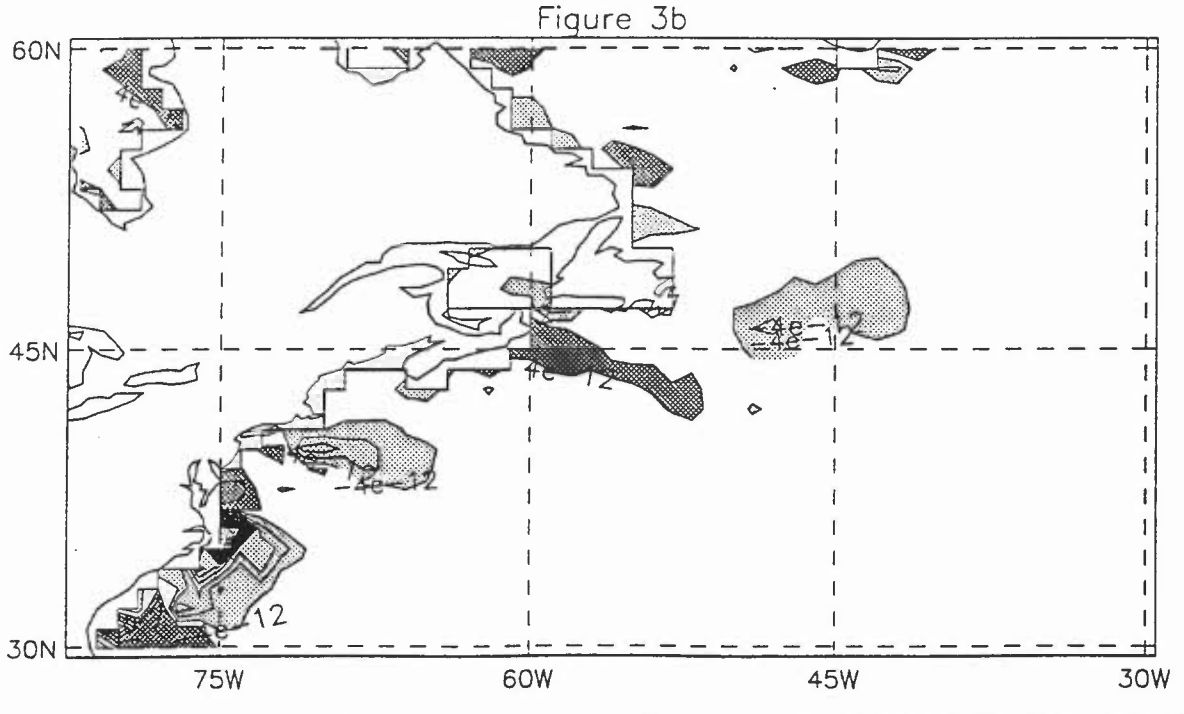

Figure 3: Monthly mean values corresponding to figure 2 of (a) J(ψ,f/H) the barotropic flow across f/H contours (see (7) and (b) JEBAR for the third month of integrationof FOAM. The contour interval is 8 10^{-12} s^{-2}. See text for details of the smoothing of the fields.

Details of calculation of diagnostics presented

The Bryan-Cox code takes the curl of the vertically averaged rate of change of momentum to eliminate the "unknown" surface pressure so that the rate of change of the barotropic streamfunction can be calculated. The vorticity diagnostics presented in the next section were calculated by picking off the terms in the components of the momentum equation as they were calculated (in subroutine CLINIC) on each timestep. The vertical integral and vertical average of each of the five terms was calculated and the curl of each of these terms evaluated using the finite difference formulation of the curl used by the Bryan-Cox model. The results were then added to accumulating totals. Thus the nonlinear terms are calculated exactly as they are appear in the model; using instantaneous fields and omitting the metric terms (uv tan ϕ and u^2 tan ϕ) which are not included in the Bryan-Cox model. Because the surface pressure is not immediately available in the model, the bottom pressure torque is calculated as a special case; by subtracting the four other terms from the curl of the rate of change of vertically averaged momentum (i.e. the curl of the vertical average of the left hand side of (1)).

Diagnostics of the vorticity tendency are particularly sensitive to small scale motions and grid scale noise. To make the plots more legible the fields displayed have been smoothed by several applications of the Laplacian of the field itself. To be precise if F is the original field, smoothed fields F^i are given by

$$\begin{aligned} F^0 &= F \\ F^{i+1} &= F^i + \omega\nabla^2 F^i \quad \text{for } i \geq 1 \ . \end{aligned} \tag{10}$$

In all the plots presented ω is chosen so as to reduce two gridlength noise by a factor of 0.2 on each iteration and F^5 or F^{10} is presented. For a given contour interval, c, contours are plotted for the values c/2 + n c (n being an integer) and areas where values are larger than c/2 are darkly shaded and areas where values are less than -c/2 are lightly shaded.

3. Results of diagnostic calculations

The first set of vorticity diagnostics (the curl of the vertically meaned tendencies) are dominated by the Coriolis (8) and JEBAR contributions. Figure 3 presents the monthly mean values of these fields from the same month of the integration as used in figures 1 and 2a. A smaller area than used in figures 1 and 2 has been chosen to aid legibility and the fields have been smoothed by 10 applications of the weak Laplacian smoother (10). The contour interval is 8 10^{-12} s^{-2}. The largest contributions occur, of course, near the coast and near the continental slope where the variations in f/H are sharpest. Large contributions occur near 45 °N, 45 °W in the region of the Flemish Cap.

In order to investigate departures from a simple local balance between the JEBAR and Coriolis contributions, the sum of these two terms is presented in figure 4 (a) with the contributions from the "viscous torque" (4(b)), wind stress curl (4(c)) and advection term (4(d)). Note that the

Figure 4a

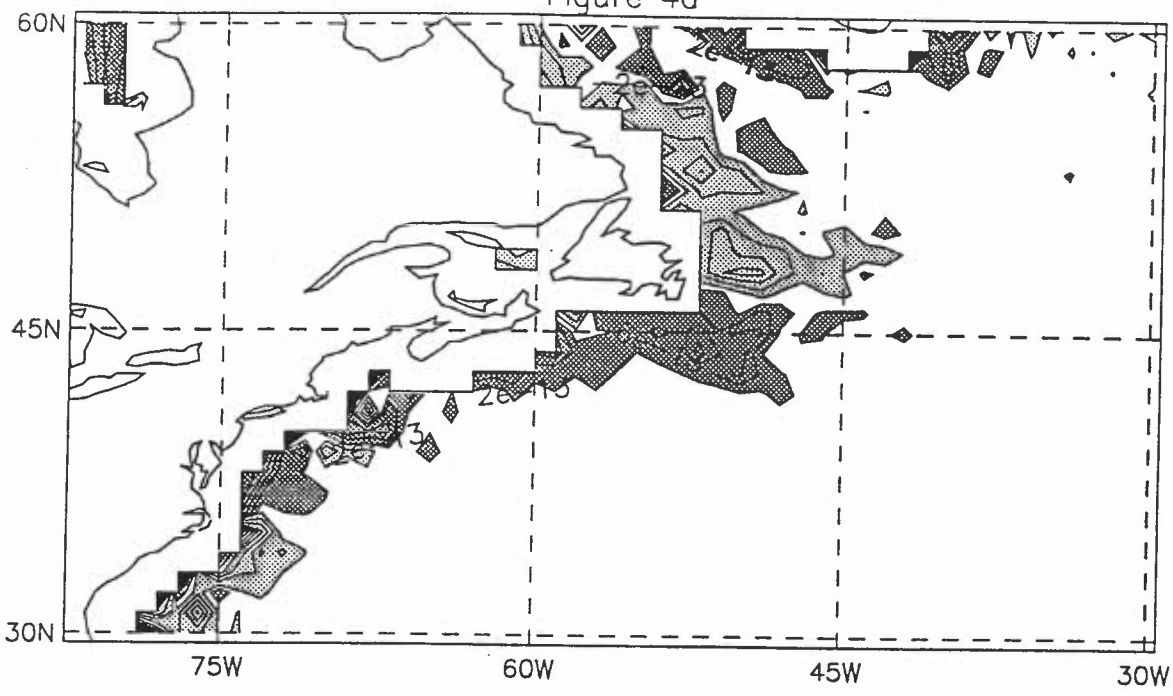

Figure 4b

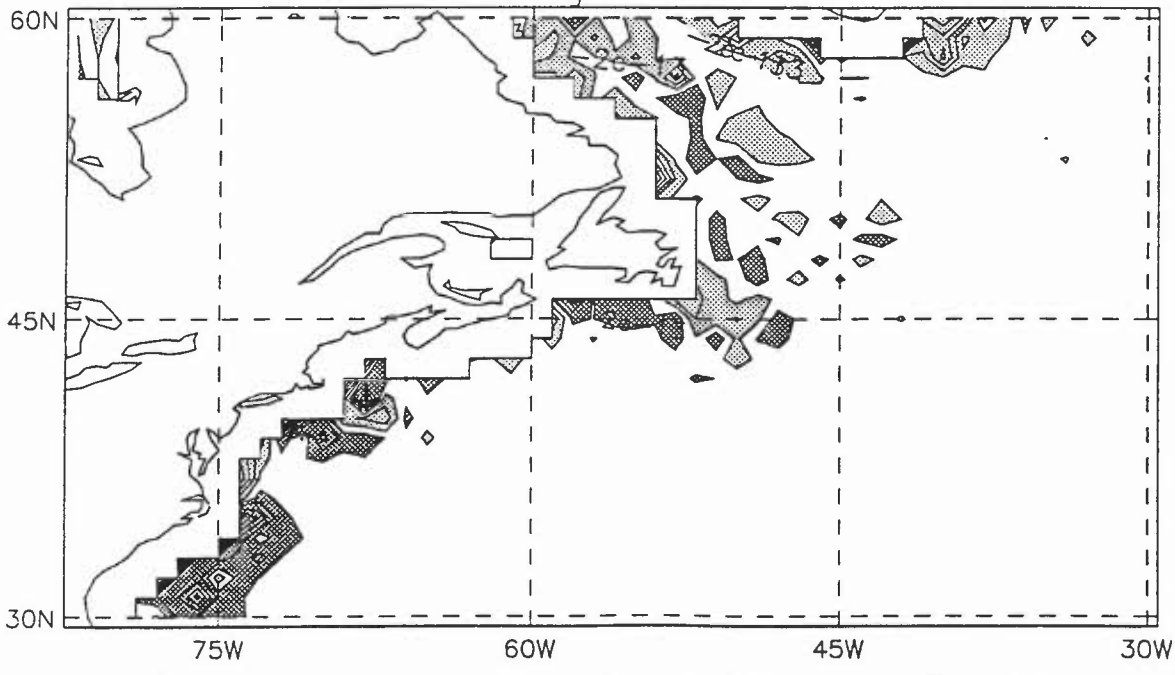

Figure 4: Monthly mean values corresponding to figure 2 of the first set of vorticity diagnostics at interior ocean points: (a) JEBAR + J(ψ,f/H) (b) viscous torque (c) the curl of the wind stress and (d) the curl of the non-linear advection. The contour interval is 4 10^{-13} s^{-2} in all plots. The fields have been smoothed 10 times using (9) with $\omega = 0.2$.

Figure 4c

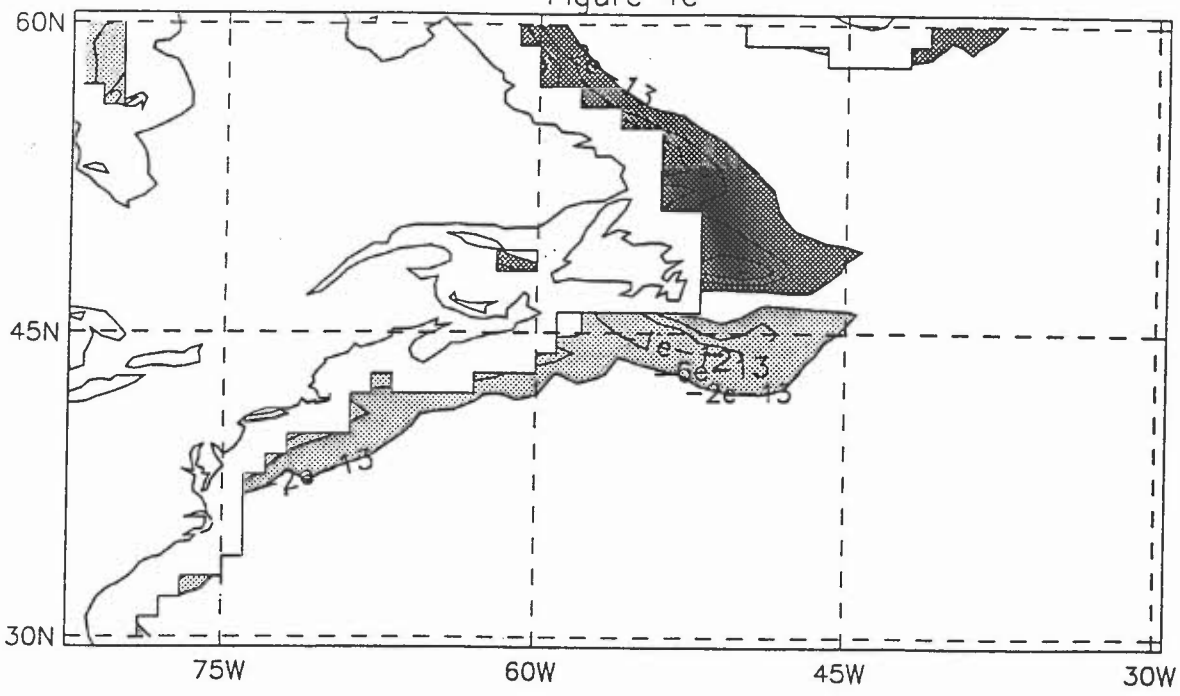

Figure 4d

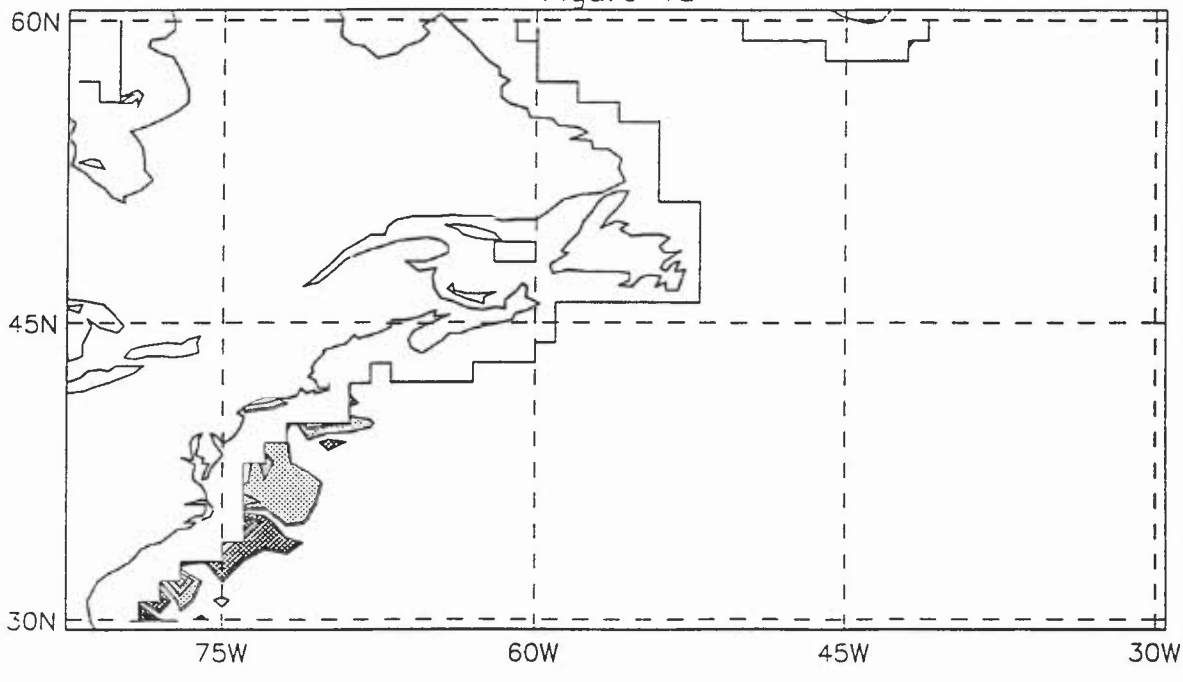

contour interval in figure 4 is ten times smaller than that in figure 3. Figure 4 shows that the wind stress curl in the FOAM model largely balances the residual of the Coriolis and JEBAR contributions in the regions of the Labrador current, Mid-Atlantic Bight and south of the Grand Banks, though the "viscous torque" is not completely negligible in these regions. Near Cape Hatteras the viscous torque (4(b)) balances the residual with a smaller, but not negligible, contribution from the advection (4(d)).

The coastlines in figures 3 and 4 differ for a reason which is worth explaining. The Bryan-Cox model solves an elliptic equation for the rate of change of the barotropic streamfunction, which is derived from the curl of the depth average of (1) and includes contributions from JEBAR . To satisfy the no-slip and no-normal flow boundary conditions at an island boundary, the streamfunction is specified to take the same value at all points in the island **and** at all ocean tracer points adjacent to the island, that is on the island perimeter. The streamfunction value on the island is adjusted, much like the points in the ocean interior, so that it fits the source function at these perimeter points. The streamfunction on the main continent in the model (which includes America, Asia and Africa) is set to zero and no adjustment of the streamfunction is made to fit the streamfunction at its perimeter points. Consequently JEBAR and the Coriolis (8) contributions do not balance at these perimeter points. They are not shown in figure 4 because they lie off the scale of the plot. It is not clear how important this inconsistency is but it is another reason for using a surface pressure formulation rather than a streamfunction formulation (Killworth et al 1991, Dukowicz & Smith 1994).

Figure 5 presents the main contributions to the second set of vorticity diagnostics (the curl of the vertically integrated tendencies). The contour interval is 10^{-9} cm s^{-2} and the fields have been smoothed by five iterations of the filter (10). The bottom torque ((6) and figure 5a) and Coriolis term ((9) and figure 5b) are generally of similar magnitude and opposite sign. Unlike the first set of diagnostics, the viscous torque (figure 5c) is comparable in amplitude with the first two contributions in many regions, particularly near Cape Hatteras and in the Labrador basin. The sum of the bottom torque and viscous torque, figure 5d, is in close balance with the Coriolis term (Sverdrup transport, figure 5b). Comparison of figures 5a, 5c and 5d show that small-scale noise in the bottom torque and viscous torque fields are strongly anti-correlated. This is even more pronounced in colour plots (not shown) of gridpoint values of the unfiltered fields.

Figure 6(a) presents the contribution of the advection term using the same contour interval as figure 5. The main point is that in a model of 1° resolution the advection contribution is not completely negligible near the true Gulf Stream separation point, but that it is not the dominant contribution even in this region. The contribution shown in figure 6(a) uses formulation D of the momentum flux (Bell 1997) with weak smoothing of the streamfunction to avoid noise in the momentum fluxes. Figure 6(b) presents the contribution from the wind stress curl using a contour interval ten times smaller than that of figures 5 and 6(a). Here the main point is that the wind stress curl plays little role in the **local** vorticity balance, at least in the Labrador Sea and near the western boundaries. The wind stress curl takes the same sign over large regions so that its integrated effect on the streamfunction (the Sverdrup transport) is of course significant. This point, that the integrated effect of each of the contributions on the streamfunction is not clear

Figure 5a

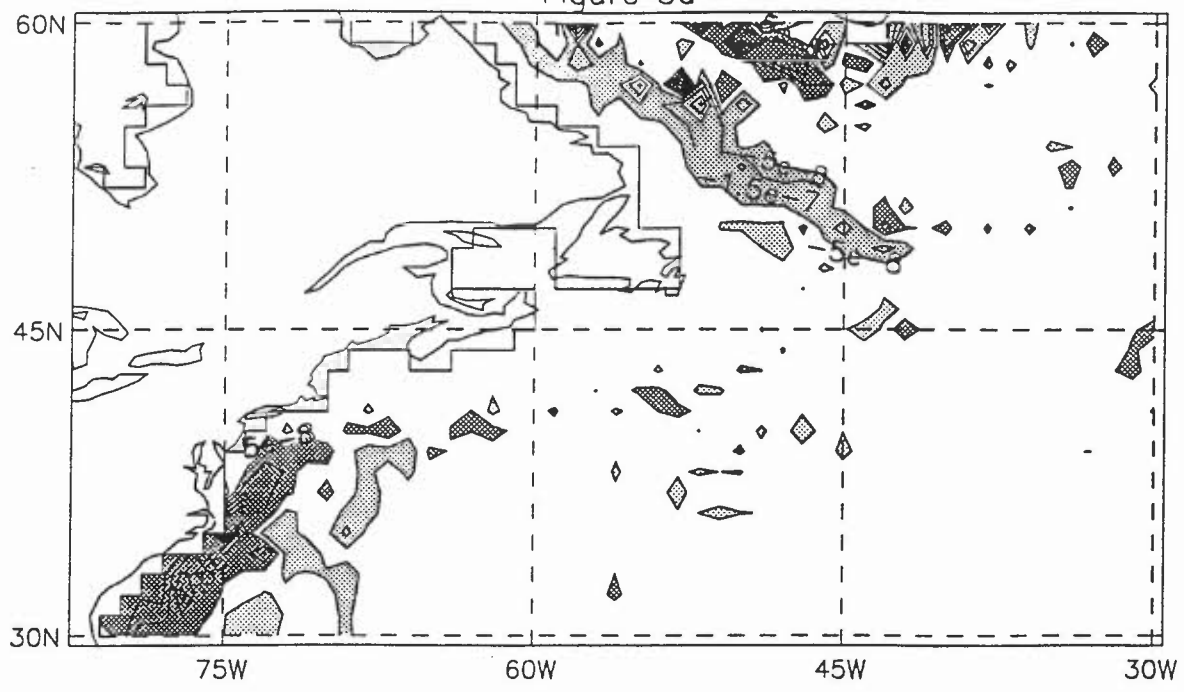

Figure 5b

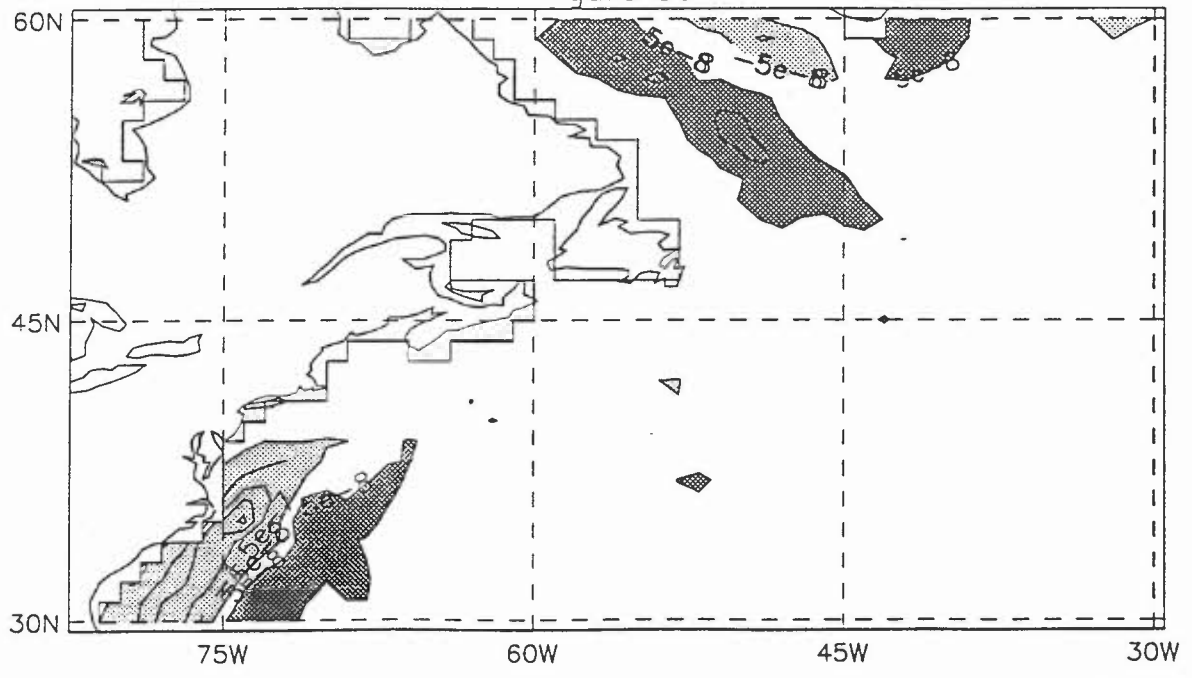

Figure 5: Monthly mean values corresponding to figure 2 of the second set of vorticity diagnostics: (a) the bottom pressure torque (b) $-\beta V$ (c) the viscous torque and (d) the viscous torque plus the bottom pressure torque. The contour interval is 10^{-7} cm s^{-2} in all plots. The fields have been smoothed 5 times using (9) with $\omega = 0.2$.

Figure 5c

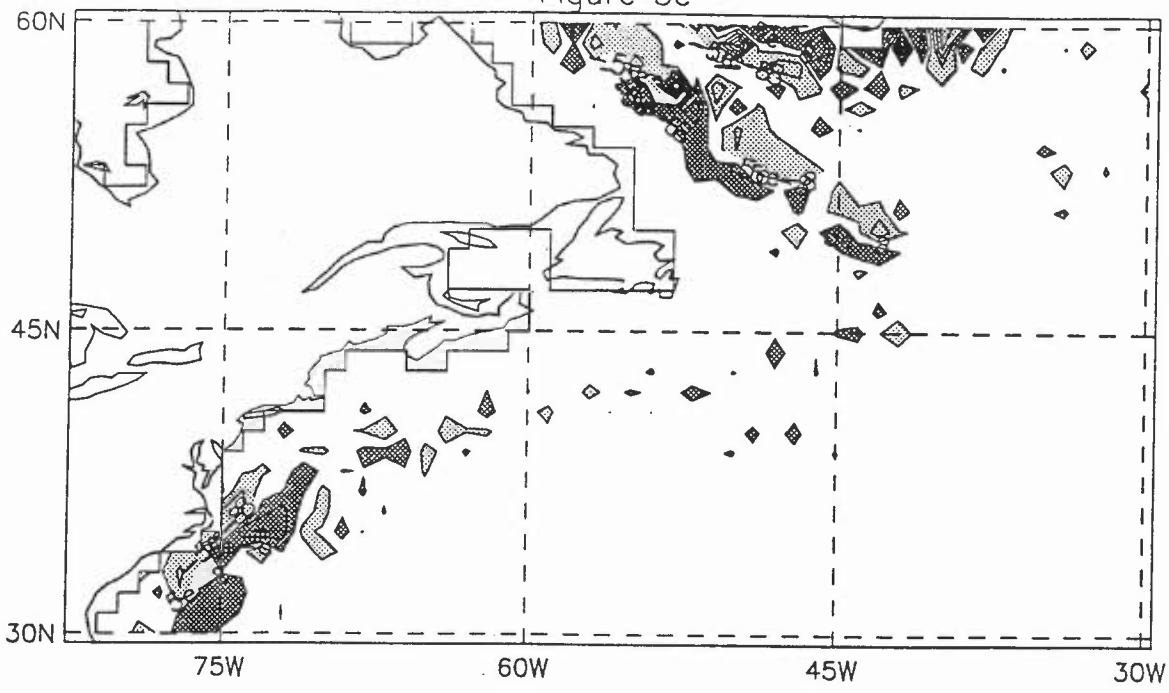

Figure 5d

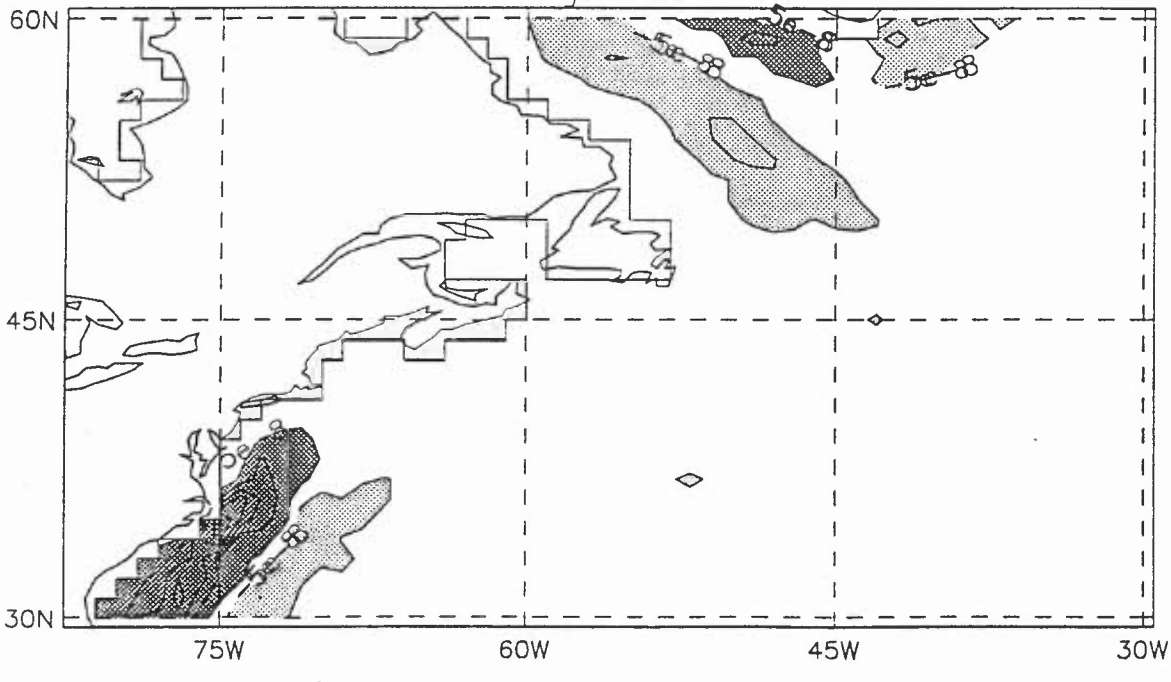

Figure 6a

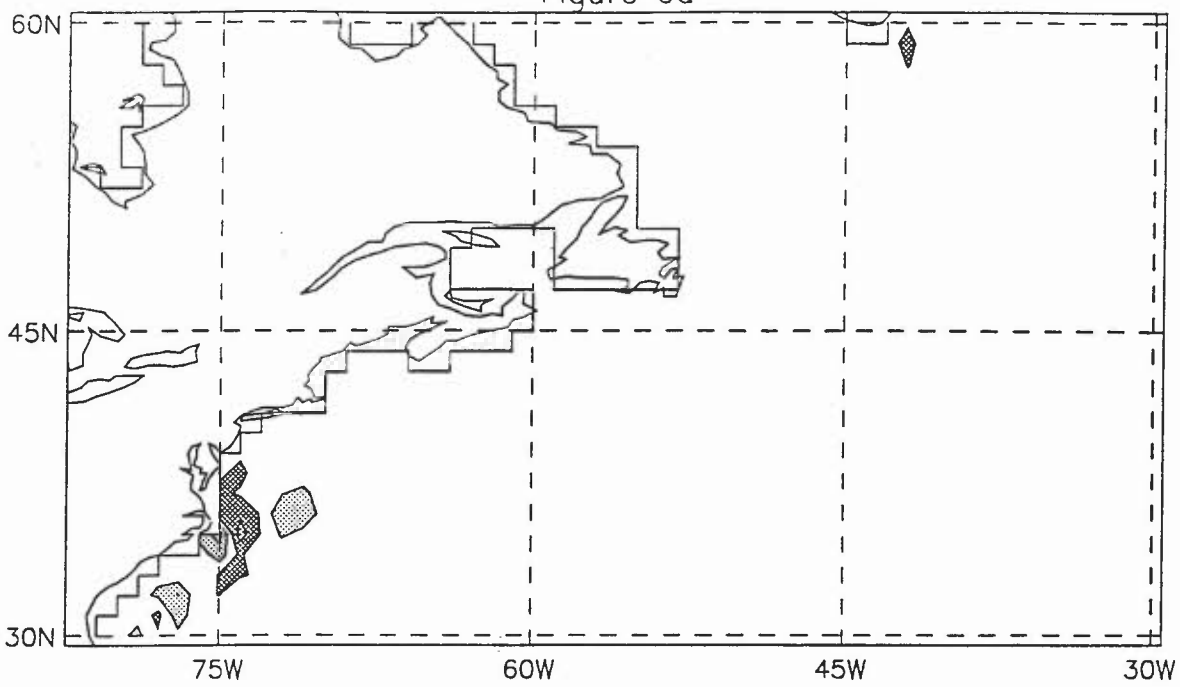

Figure 6b

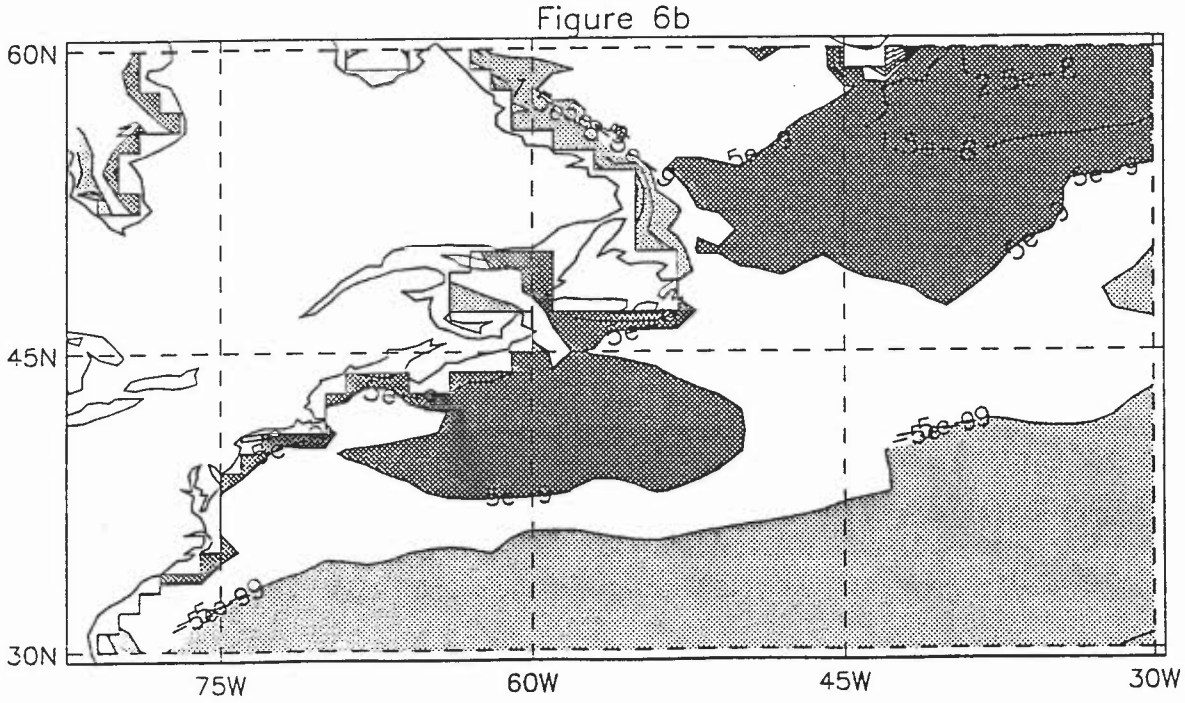

Figure 6: Monthly mean values corresponding to figure 2 of the second set of vorticity diagnostics: (a) the curl of the non-linear advection (b) the curl of the wind stress. The contour interval in (a) is 10^{-7} cm s^{-2} (the same as in figure 5) and in (b) is 10^{-8} cm s^{-2}. The fields have been smoothed 5 times using (9) with $\omega = 0.2$.

from figures 3-6, is explored further in section 5.

4. Vortex stretching and bottom torques in the Bryan-Cox model

The results presented in section 3 confirm the findings of previous authors, already cited, who have emphasized the importance of the bottom torque in the ocean circulation. Guided by the dominance of the Sverdrup transport and the bottom pressure torque terms in the second set of vorticity diagnostics, and the fact that the viscous torque is not negligible, this section considers the representation of the corresponding terms in the third set of vorticity tendency diagnostics as they appear in the finite difference form used by the Bryan-Cox code. In a quasi-geostrophic model the bottom pressure torque and the vortex stretching are identical. More generally the second and third sets of vorticity diagnostics are closely related and the bottom pressure torque and vortex stretching terms have clearer physical significance than the JEBAR term. In an ocean which is basically barotropic the JEBAR term can be used to interpret the flow but in a baroclinic ocean in which the bottom flow is quite different from the vertical mean flow the main use of JEBAR is as a computational device.

The Bryan-Cox code stores the model variables on the B grid as illustrated in figure 7. The two components of velocity (u, v) are stored at the points marked ✖ and the tracers and (implicitly) the pressure at the points marked ● . The index i denotes the model column and j the model row. The longitude λ depends on i and the latitude ϕ on j. $\Delta\lambda$ and $\Delta\phi$ denote the grid spacing. The tracers are stored at points with integer values of i and j and the velocities at points with half integer values.

Using the notation of Cox (1984) the reduced form of the momentum equation which will be considered is:

$$\begin{aligned} 0 &= fv + G_\lambda \quad ; \quad G_\lambda = -\frac{1}{\rho_0 a \cos\phi}\overline{\delta_\lambda p}^{\phi} + F_\lambda \\ 0 &= -fu + G_\phi \quad ; \quad G_\phi = -\frac{1}{\rho_0 a}\overline{\delta_\phi p}^{\lambda} + F_\phi \ . \end{aligned} \tag{11}$$

As discussed above the non-linear advection and wind stress forcing terms have been neglected in (11). The total force per unit mass (G_λ , G_ϕ) has been introduced for convenience in the arguments below. The averaging ($\overline{\ }^{\phi}$) and finite difference operators (δ_ϕ) in (11) are given by:

$$\begin{aligned} \overline{\mu}^{\phi}_{i,j} &= \tfrac{1}{2}(\mu(i,j+\tfrac{1}{2}) + \mu(i,j-\tfrac{1}{2})) \\ \delta_\phi \mu_{i,j} &= (\mu(i,j+\tfrac{1}{2}) - \mu(i,j-\tfrac{1}{2})) \ / \ \Delta\phi \end{aligned} \tag{12}$$

Similar expressions apply for averages and differences in λ.

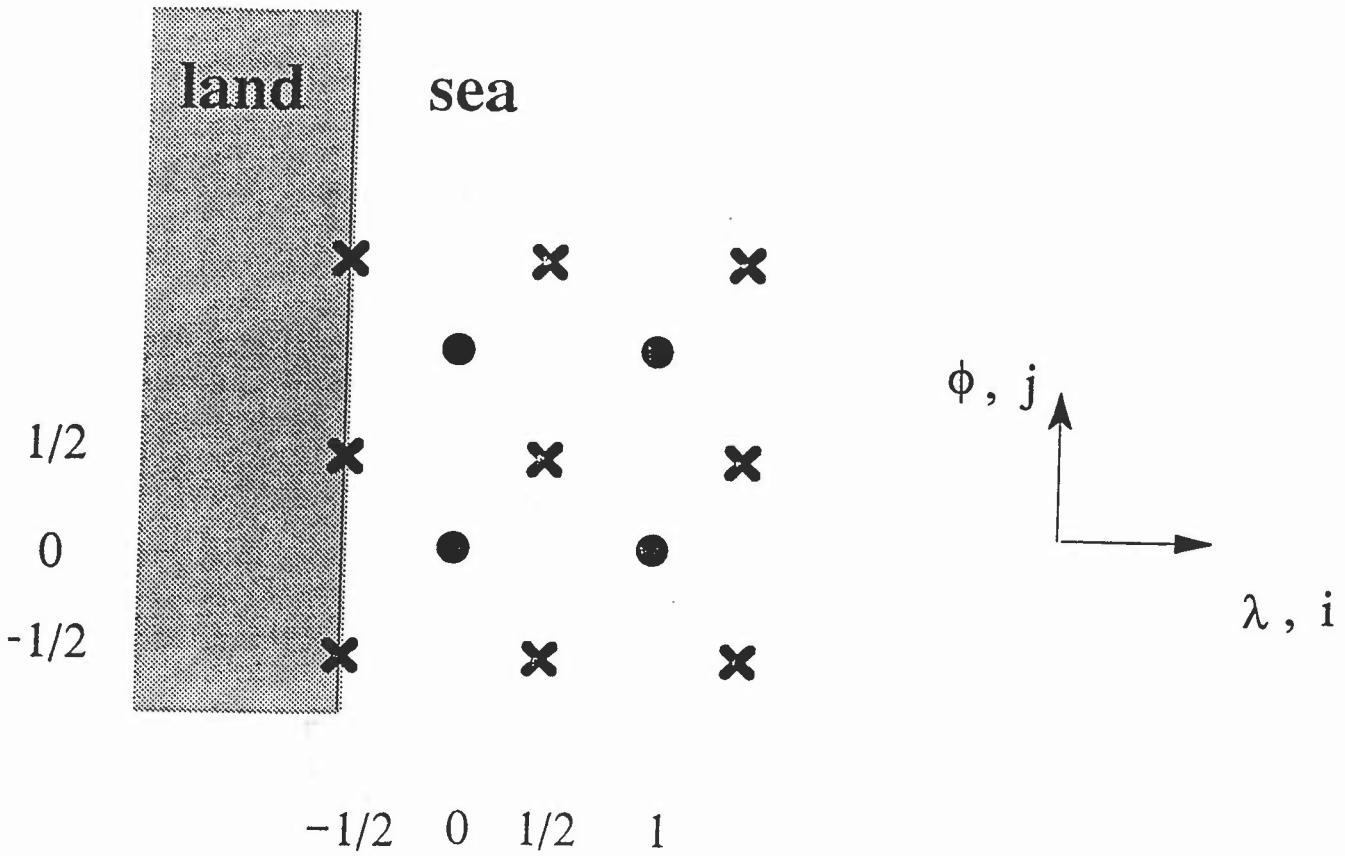

Figure 7: The horizontal structure of the grid used by the Bryan-Cox model. Tracer, streamfunction and pressure values are stored at the points marked ● and horizontal velocities u and v at the points marked ✖. A land boundary is marked for i=-½.

Some important expressions for individual terms in the third set of diagnostics, as they apply to a continuous fluid, have close analogues in the finite difference form used by the Cox model. Firstly there is a close analogue for the standard expression for the Coriolis term. Taking the curl of (1) using (2) the Coriolis terms for a continuous fluid result in a Sverdrup transport and a vortex stretching term:

$$\begin{aligned} curl(fv,-fu) &= -\frac{f}{a\cos\phi}(\partial u/\partial\lambda + \cos\phi\,\partial v/\partial\phi) - \beta v \\ &= f\,\partial w/\partial z - \beta v \ . \end{aligned} \qquad (13)$$

The form of the curl used by the Cox model is evaluated at tracer points and is given by

$$curl(a_\lambda, a_\phi) = \frac{1}{a\cos\phi}\left\{\frac{1}{\Delta\phi}\overline{(\delta_\lambda a_\phi)\Delta\phi}^{\phi} - \frac{1}{\Delta\lambda}\delta_\phi(\overline{a_\lambda\Delta\lambda}^{\lambda}\cos\phi)\right\} \ . \qquad (14)$$

Taking the curl of the Coriolis terms one can rearrange the terms to give

$$curl(fv,-fu) = -\frac{\overline{f}^{\phi}}{a\cos\phi}\{\frac{1}{\Delta\phi}\delta_{\lambda}\overline{u\Delta\phi}^{\phi} + \frac{1}{\Delta\lambda}\delta_{\phi}(\overline{v\Delta\lambda\cos\phi}^{\lambda})\} - \frac{\delta_{\phi}f}{a\cos\phi}\{\frac{\Delta\phi}{4}\delta_{\lambda}\delta_{\phi}(u\Delta\phi) + \frac{1}{\Delta\lambda}(\overline{v\Delta\lambda\cos\phi}^{\lambda\phi})\}. \quad (15)$$

The first term in (15) includes the divergence of the horizontal velocity, as it is calculated by the model, and hence corresponds precisely to the first term in (13). Thus the Bryan-Cox code has a precise analogue of vortex stretching. The second half of the other term in (14) is an accurate analogue of the Sverdrup transport, $-\beta v$, whilst the first half of that term is an error term which is of order $(\Delta\phi)^2$ smaller than the other term and hence negligible for good resolution.

A second analogue of the continuous equations in the Cox model's formulation of the third set of vorticity diagnostics is that the curl of the pressure gradient is identically zero in the interior of the model (providing the grid spacings $\Delta\phi$ and $\Delta\lambda$ are uniform). For from (11) and (12)

$$curl(\overline{\delta_{\phi}p}^{\lambda}, \frac{1}{\cos\phi}\overline{\delta_{\lambda}p}^{\phi}) = \frac{1}{a\cos\phi}\{\frac{1}{\Delta\phi}\delta_{\lambda}\overline{\delta_{\phi}p}^{\lambda\Delta\phi}{}^{\phi} - \frac{1}{\Delta\lambda}\delta_{\phi}\overline{\delta_{\lambda}p}^{\phi\Delta\lambda}{}^{\lambda}\} \quad (16)$$

which is zero when the grid spacings are uniform.

A third analogue concerns the forces implied by the model formulation at velocity points lying on the land/sea boundary. The velocity at these points is always zero, so the acceleration is zero and by Newton's second law the total force on these points should be zero. The curl of the force on the topography can then be calculated by evaluating the curl of the total force per unit mass and setting the total force per unit mass at land points to zero. (It may be helpful to remark that the formula (11) for the total force makes implicit assumptions about the stress tensor which are only appropriate for a fluid and should not be employed at land points. Thus (16) does not apply at tracer points bordering ocean points.)

For simplicity consider the north-south coastal boundary shown in figure 7 in which the velocity points on the coast are at column i=-1/2. Taking the height of the topographic step at i=1/2 to be ΔH, the curl of the total force on the cell centred at the tracer point i=0, j=0 is

$$\Delta H\ curl(G_{\lambda},G_{\phi}) = \frac{\Delta H}{a\cos\phi}\{\frac{\overline{G_{\phi}}^{\phi}}{\Delta\lambda} - \tfrac{1}{2}\,\delta_{\phi}(G_{\lambda}\cos\phi)\}\Big|_{i=\frac{1}{2},j=0} \quad (17)$$

in which the term on the right hand side is evaluated at i=1/2, j=0. The curl of the "pressure"

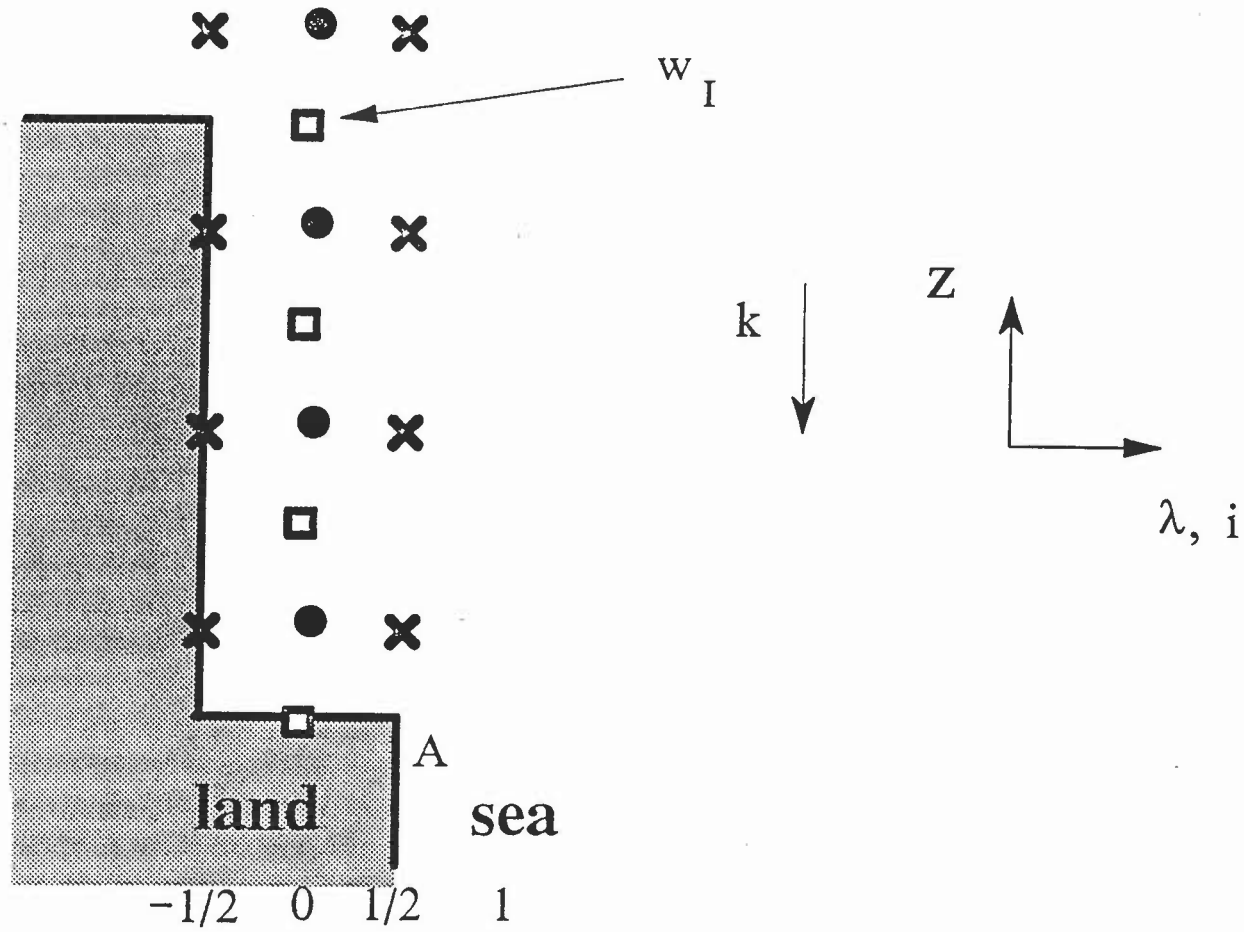

Figure 8: The vertical structure of the grid used by the Bryan-Cox model. w_I, the bottom interior vertical velocity, is the vertical velocity on the tracer grid at the top edge of the topography.

force on the cell is then obtained by substituting expressions for the pressure gradient force from (11) into (17) and is

$$\begin{aligned} \Delta H \; curl\; /\!/ -\nabla p /\!/ \; &= -\frac{\Delta H}{a^2 \Delta\lambda \cos\phi} \{ \overline{\delta_\phi p}^{\phi\lambda} - \tfrac{1}{2}\, \delta_\phi (\overline{\delta_\lambda p}^{\phi}) \} \Big|_{i=\frac{1}{2}, j=0} \\ &= -\frac{\Delta H}{a^2 \Delta\lambda \cos\phi} \overline{\delta_\phi p}^{\phi} \Big|_{i=0, j=0} \end{aligned} \qquad (18)$$

which is a precise analogue of J(H,-∇p) the bottom pressure torque (for the simple case considered in which $\partial H/\partial\phi = 0$).

A less satisfactory aspect of the Bryan-Cox code's representation of the third set of vorticity diagnostics concerns the stepped nature of the topography in the model. For the rigid-lid version of the code the vertical velocity at the tracer points at the bottom of the model is identically zero.

Thus the vortex stretching integrated over a full water column is identically zero despite the fact that above the topographic steps the code represents vortex stretching accurately. A useful approximate relationship between the vertical motion near the bottom of the model and the bottom torque is obtained by taking the curl of (11) and integrating over the tracer cells which are adjacent to the topographic steps as illustrated in figure 8. Then using (15)

$$\sum_{STEP} curl(G_\lambda, G_\phi)\ \Delta z = (-fw_I + \sum_{STEP} \beta v \Delta z) \qquad (19)$$

The term on the l.h.s. of (19) represents the curl of the force on the topography. w_I, which is the vertical velocity at the top edge of the topography as illustrated in figure 8, will be termed the interior bottom vertical velocity. The final term in (19) is the contribution to the Sverdrup transport from grid boxes adjacent to the topographic step.

As it stands (19) suggests that the formulation of vorticity dynamics in the Bryan-Cox model is quite good. As the vertical and horizontal resolution of the model improve, the final term in (19) (the partial integral of the Sverdrup transport) should become negligible and the bottom torque faithfully related to near bottom vertical velocities.

Figure 9(a) illustrates $-fw_I$. Holland (1973 figure 5) presented a simple conceptual model of the flow up continental shelves driven by thermal wind shear which is useful for interpreting figure 9(a). The north-south thermal gradient between 30 and 45 °N is associated with a zonal thermal wind shear with flow increasing westward with depth. In the absence of a special adjustment of the vertically averaged flow the flow at the bottom will be westward and thus up the continental slope and down the western side of the mid-Atlantic ridge, in agreement with figure 9(a). There is also, in the FOAM model at least, sinking of the cold water from the shelf down the continental slope. The vertical velocities in Bryan-Cox models are determined by the horizontal velocities and conservation of volume (or mass). Thus despite the fact that there is no smooth bathymetric slope for the fluid to follow one might expect the model to represent w_I reasonably accurately.

Figure 9(a) can be compared with the bottom and viscous torques presented in figures 5(a) and 5(d) though the contour interval is smaller in figure 9 than figure 5. To facilitate assessment of (19), figure 9(b) presents the sum of fw_I and the bottom pressure torque and figure 9(c) the sum of fw_I and the total torque on the bathymetry. The latter is the sum of the bottom pressure torque and the viscous torque on the bathymetry which is calculated by integrating the curl of the viscous force only over grid boxes adjacent to the steps. Figures 9(b) and 9(c) should be compared with 9(d) which presents the final term in (19), namely the contribution to the Sverdrup transport from grid boxes adjacent to topographic steps.

If the viscous torques were negligible and the model satisfied (19) then figures 9(b) and 9(d) would be identical. Clearly this is not the case. The agreement between figures 9(c) and 9(d) on the other hand, though not perfect, is rather good when the magnitude of the contributing fields and the neglect of the non-linear advection terms (c.f. figure 6(a)) are borne in mind. Thus it

Figure 9a

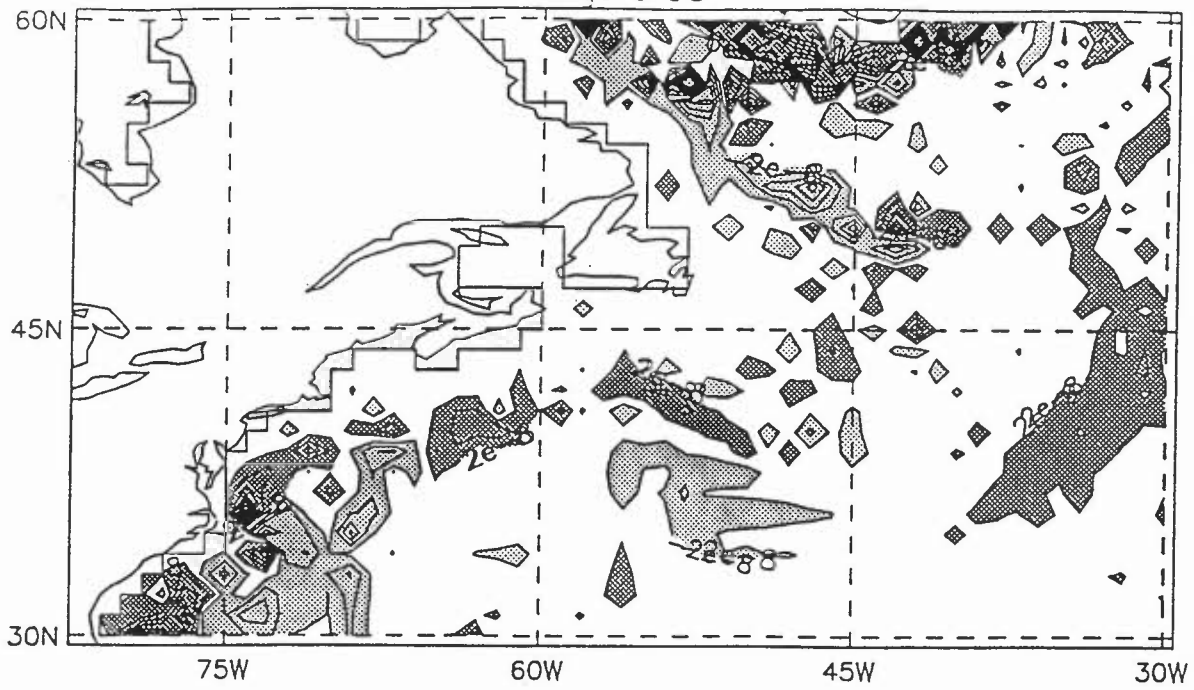

Figure 9b

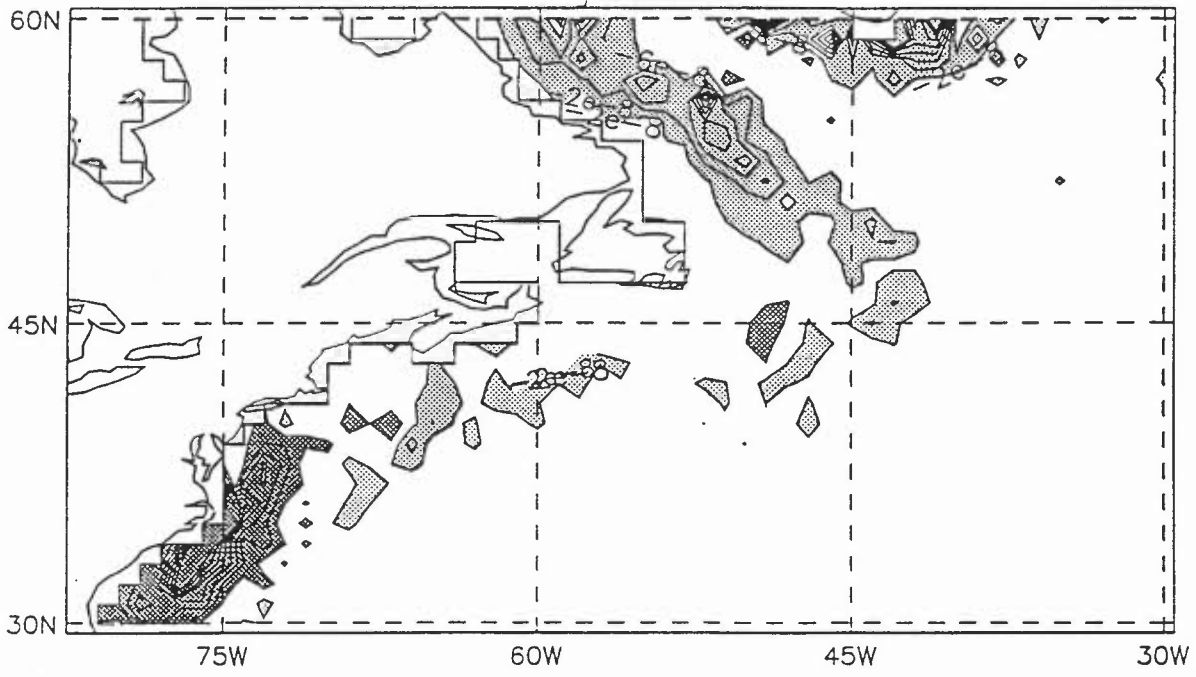

Figure 9: Monthly mean values corresponding to figure 2 of (a) - f w_I (b) f w_I + bottom pressure torque (c) f w_I + bottom pressure torque + viscous torque (d) the integral of the Sverdrup transport next to the topographic step (see (18)). The contour interval in all plots is 4 10^{-8} cm s^{-2}. The fields in (a) - (c) have been smoothed 5 times using (9) with $\omega = 0.2$.

Figure 9c

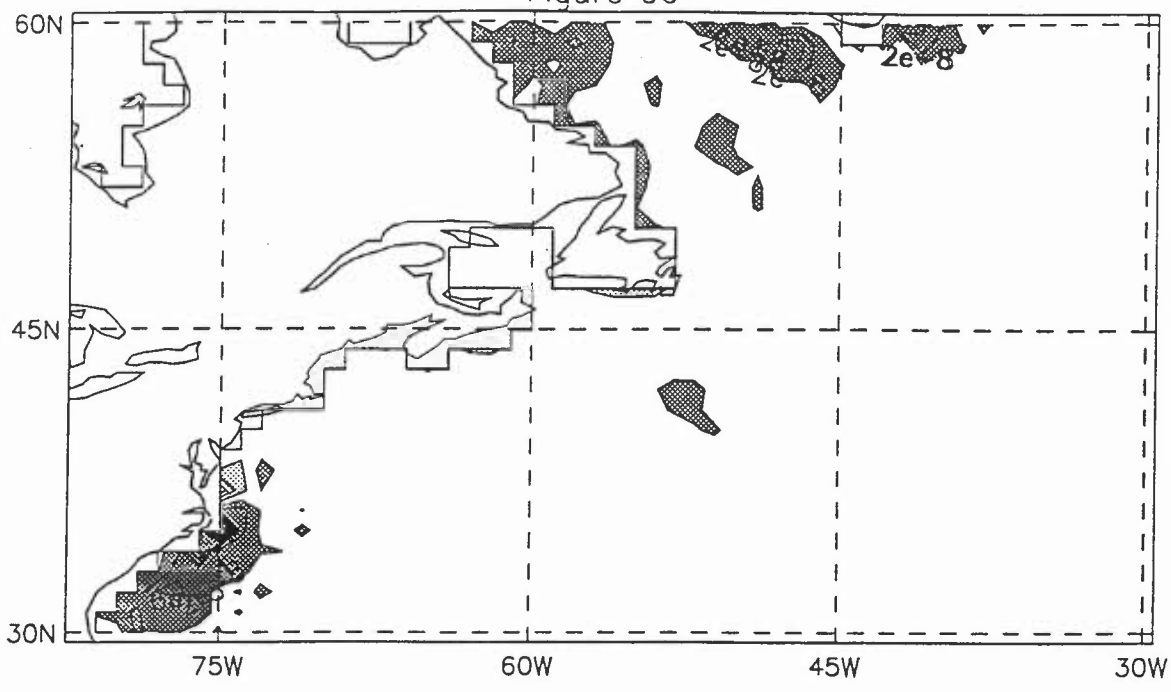

Figure 9d

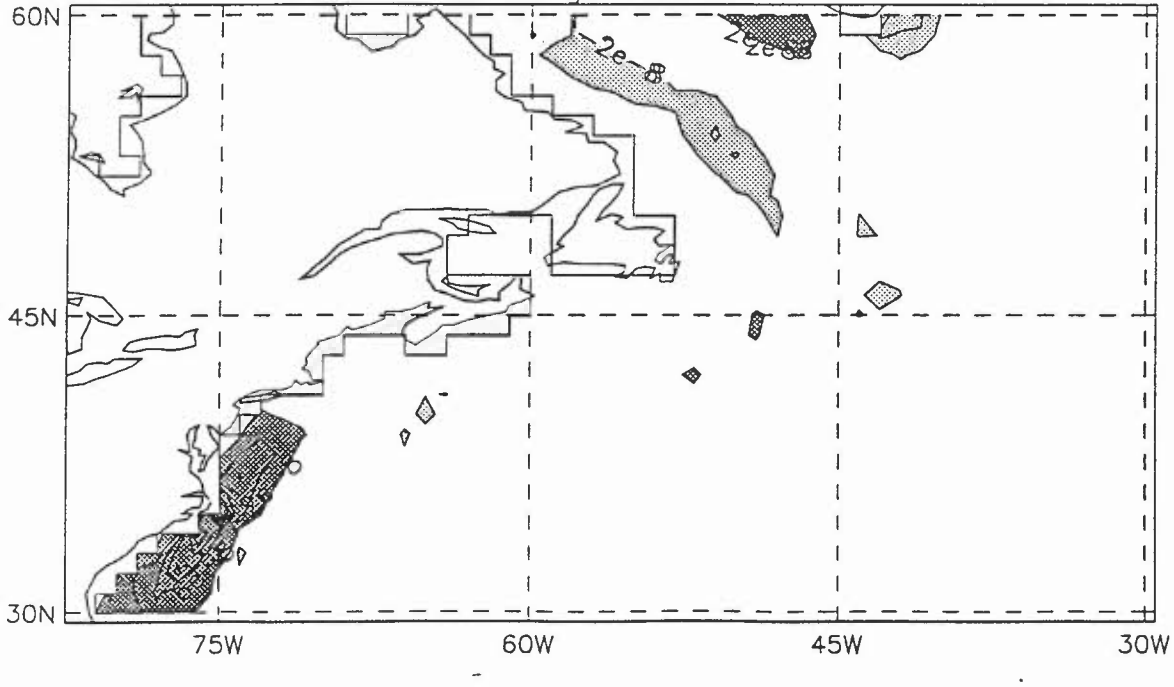

appears that the arguments leading to (19) hold quite well for the FOAM version of the Cox model.

The partial Sverdrup transport (figure 9d) accounts for some but by no means all of the difference between the bottom pressure torque and the vortex stretching (figure 9b) near the Gulf Stream separation point and in the Labrador current. Figures 9(a) and 9(b) together show that the bottom pressure torque corresponds to more rapid downwelling near Cape Hatteras, more rapid upwelling in the Labrador current and less vigorous downwelling in the northern recirculation gyre than is actually present in the interior bottom vertical velocity.

The most appropriate interpretation of the r.h.s. of (19) is not entirely clear. One interpretation is that w_I is the vertical velocity which should be at the very bottom of the model. In this case the partial integral of the Sverdrup transport would represent an error in the vortex stretching due to misplacement of the bottom vertical velocity; the vertical velocity which should be stretching the whole water column stretches only part of the water column. The interpretation of the balance of terms in (19) is also open to discussion. The large difference between the bottom pressure torque and the vortex stretching could be seen as a weakness of the model. Alternatively the close correspondence between the total torque on the bottom and the vortex stretching could be seen as a strength of the model formulation.

Hughes (1995) draws attention to a problem in the internal consistency of the JEBAR term in the Bryan-Cox model. Next to topographic steps which descend more than one vertical level, the integration by parts in the derivation of JEBAR from the potential energy of the model does not work as it does for the continuous equations. It is not clear how relevant this integration by parts is to the formulation of the bottom torque calculation. Certainly the calculation leading to (19) is quite different from that presented by Hughes and does not distinguish between single and multi-level steps in the topography. The results on the scatter in the relationship between the bottom vertical velocities and the pressure torque presented by Hughes (1995) and Wells & de Cuevas (1995 figure 3) need to be treated with some caution because the vertical velocities presented are derived from the vertical velocities on the velocity grid which are subject to a number of problems in the Cox model (Bell 1997 and Webb 1995).

5. The streamfunctions "driven" by contributions to the torque

A means of assessing the importance of the terms in (19) and the contributions to the second set of vorticity tendencies is suggested by (9). Contributions to the streamfunction, ψ, from the terms in the vorticity balance can be obtained by setting $\psi = 0$ at the eastern ocean boundary, integrating the contribution to the torque from west to east across the basin and multiplying by $-a/\beta$. This method is often used to calculate the streamfunction for the Sverdrup transport driven by the curl of the wind stress. GFGL and Myers et al (1995) use similar calculations to obtain "contributions" to the streamfunction from the terms in the first set of vorticity diagnostics by integrating around f/H contours. As the paths of integrations differ between the two sets of calculations it is clear that some caution is needed interpreting both sets of diagnostics.

Figure 10a

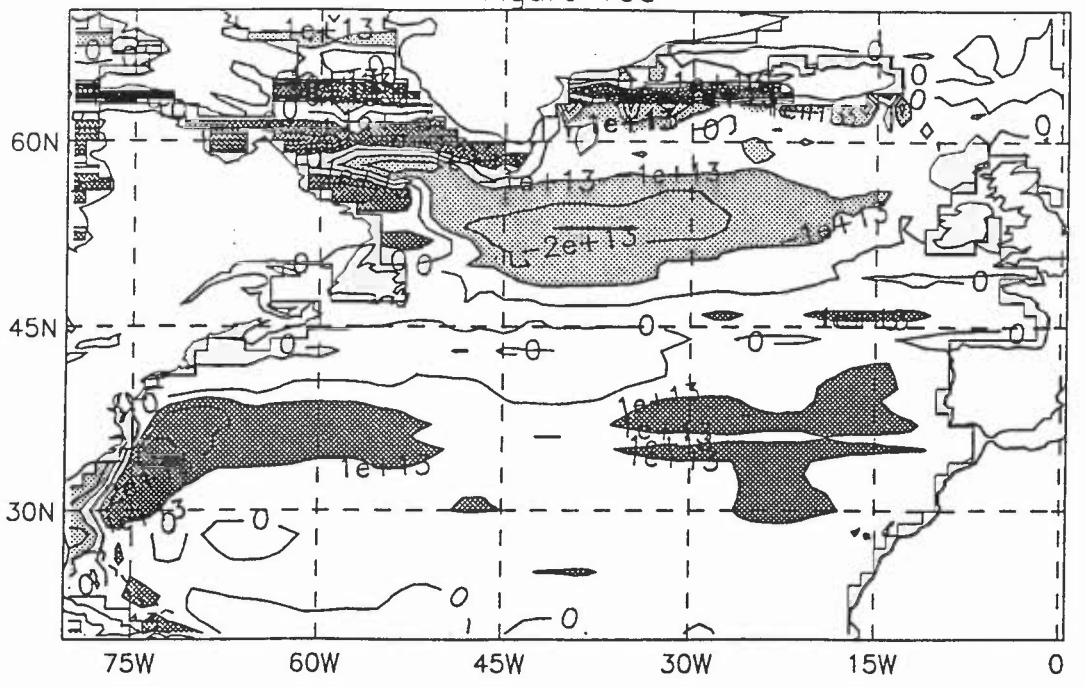

Figure 10b

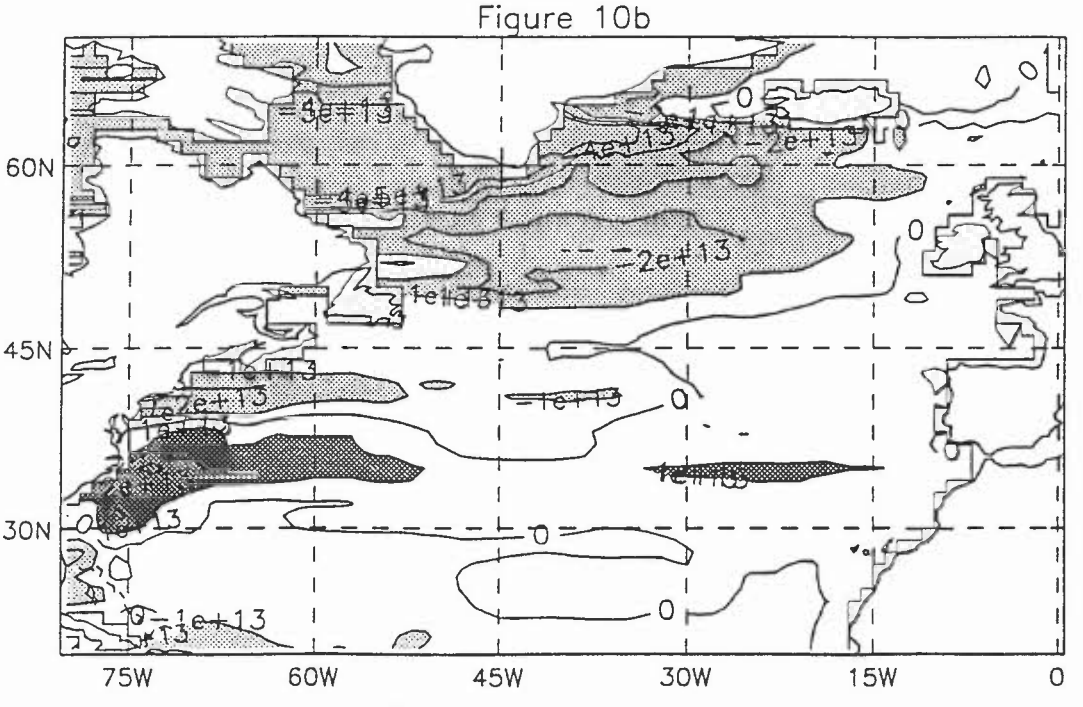

Figure 10: The contributions to the streamfunction "driven" by (a) the bottom pressure torque (b) - f w_I (c) the integral of the Sverdrup transport next to the topographic step and (d) the viscous torque on the fluid interior. The contour interval is 10 Sv in all plots.

Figure 10c

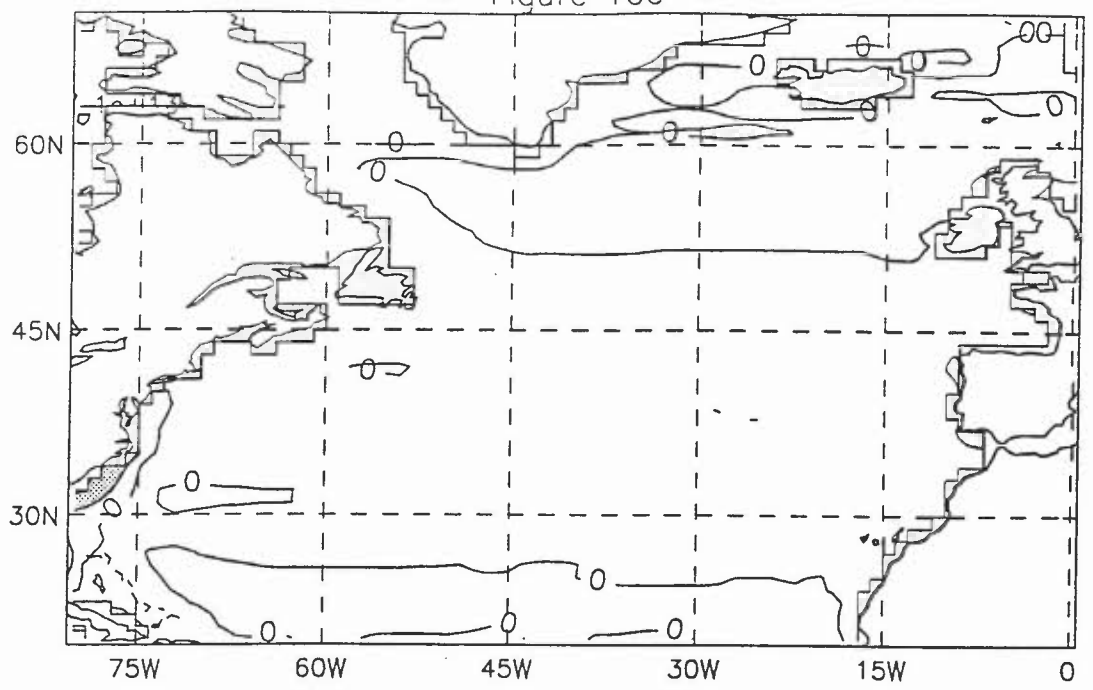

Figure 10d

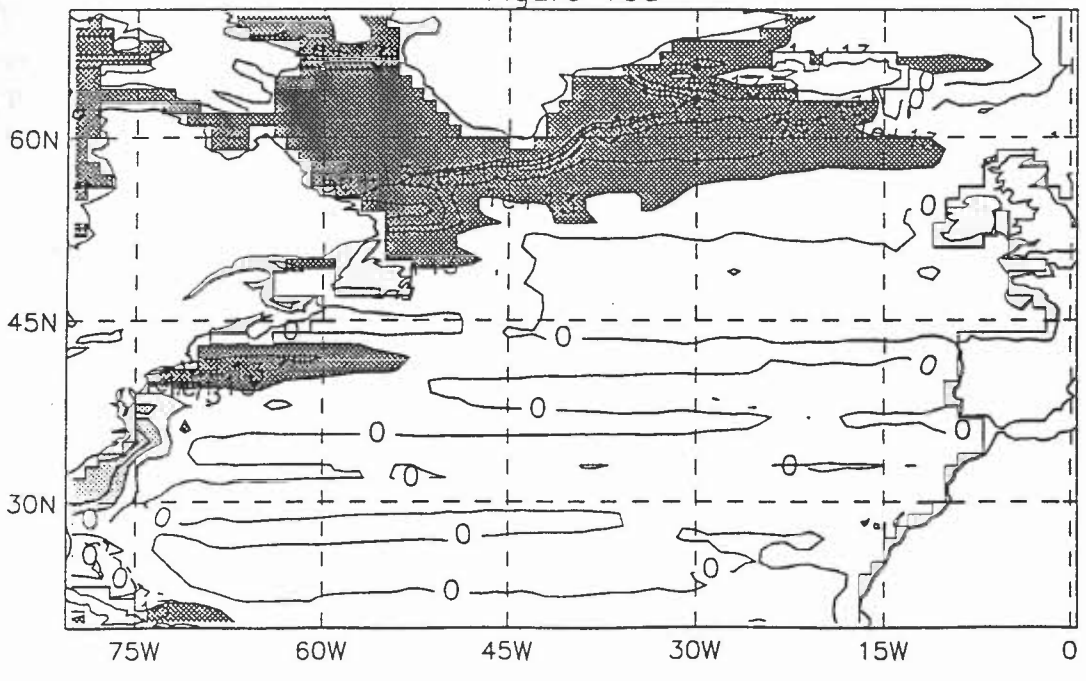

Figure 10(a) presents the streamfunction "driven" by the bottom pressure torque and figure 10(b) that driven by the interior bottom vertical velocity ($-\rho_0 f w_I$). In both cases gridpoint noise in the north south direction has been reduced in the vorticity fields by one application of a 1-2-1 filter.

Perhaps the most interesting difference between the two figures is in the Gulf Stream separation region. The streamfunction driven by the bottom pressure torque overshoots Cape Hatteras much more than that driven by the bottom velocities and the latter has a clear indication of a northern re-circulation gyre. The bottom pressure torque under-represents the flow down the continental slope in the region of the northern recirculation gyre (see figures 9(a) and 9(b)). It is this which mainly accounts for the differences between figures 10(a) and 10(b) in that region. The over-estimation of the bottom pressure torque in the region of the separation point apparent in figure 9(b) is mainly responsible for the differences between the streamfunctions in that region.

Figure 10(c) shows the streamfunction "driven" by the partial integral of the Sverdrup transport next to the step and suggests that this transport plays a relatively minor role in the FOAM model. Figure 10(d) shows the streamfunction "driven" by the viscous torque on the fluid interior - that is the viscous torque as calculated for the second set of diagnostics minus the viscous torque on the bathymetric steps. This torque drives flow into the coast north of Cape Hatteras and an anticyclonic circulation in the area of the northern recirculation gyre and appears to play a major role in the FOAM model's circulation.

It was suggested in the last section, following Holland (1973), that the bottom vertical velocities could be largely determined by the ocean's density structure, the thermal wind relation and continuity. This would then determine the contribution to the barotropic streamfunction from vortex stretching. The fact that this contribution suggests that the Gulf Stream should separate at Cape Hatteras when calculated from a model which fails to separate, seems to support this interpretation of the factors determining the barotropic circulation rather strongly.

The diagnostics presented in this paper have also been calculated for the Kuroshio current which in reality separates from the coast of Japan at about 35 °N and in the model follows the coast too far north. Figure 11 presents for this region: (a) the sum of $f w_I$ and the bottom pressure torque; (b) the streamfunction driven by the bottom pressure torque; and (c) the streamfunction driven by $-f w_I$. Figure 11(a) shows the pressure torque to exceed the vortex stretching along the whole of the coast of Honshu (the main Japanese island) and comparison of figures 11(b) and (c) show that the pressure torque drives a much stronger boundary current up the whole of the coast of Honshu than the vortex stretching.

The streamfunctions in the sub-polar gyre in figures 10(a) and (b) have a maximum transport of about 25 Sv and are in reasonable agreement with each other and GFGL figure 6. But the bottom pressure torque calculation (figure 10(b)) gives particularly poor fields in the Labrador basin. The viscous torques are particularly large and noisy in this region and to the east of Greenland (see section 3). There is little indication in either figure 10 (a) or 10 (b) of a circulation round the Flemish Cap similar to that produced by GFGL or Myers et al. (1995). Further work is needed to clarify whether this is related to the smoothing of the topography of the Flemish Cap or some

Figure 11a

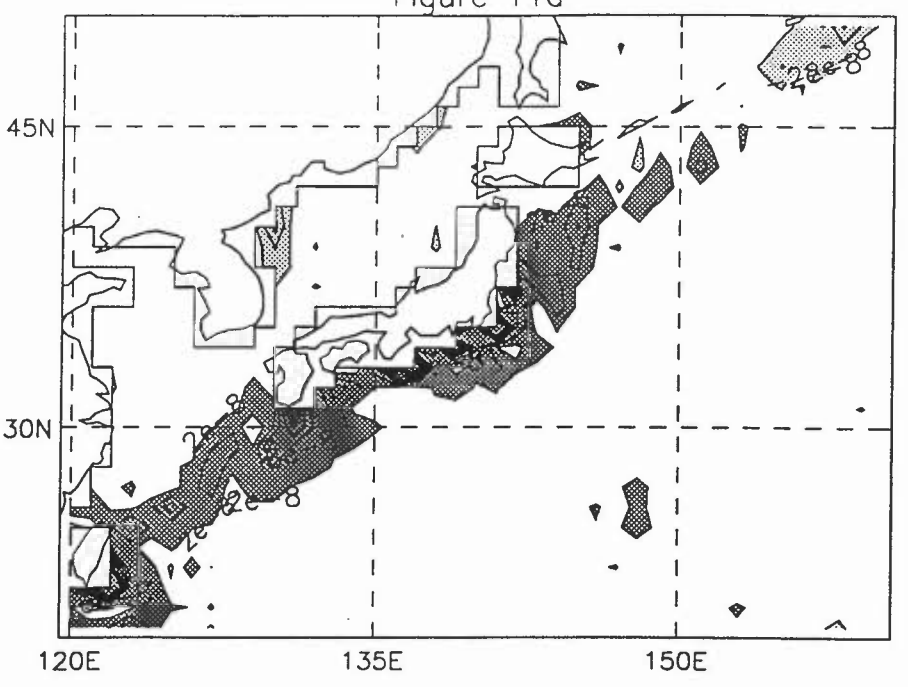

Figure 11b

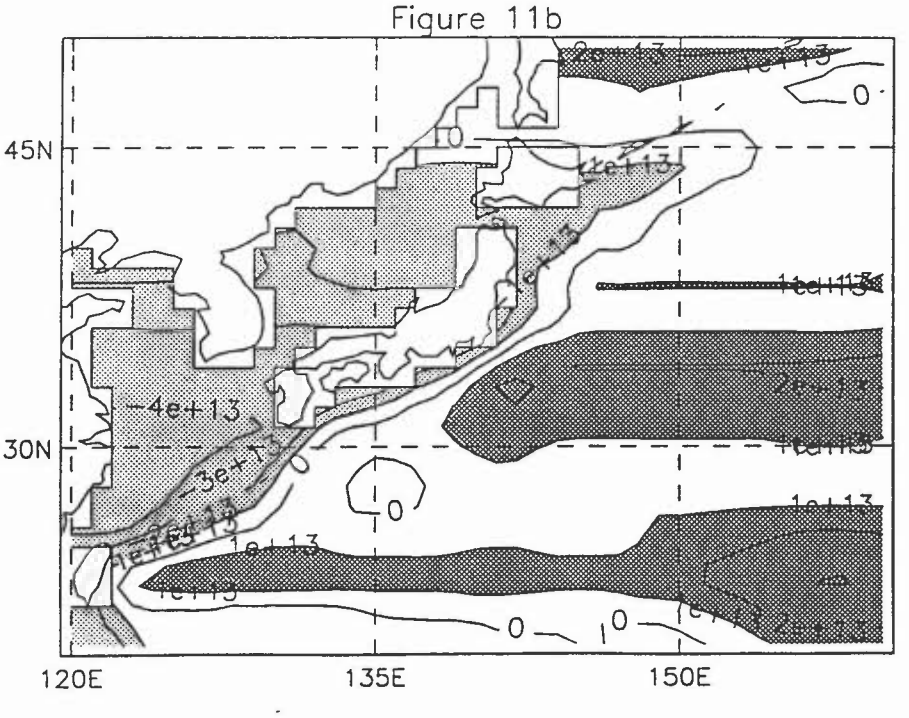

Figure 11: (a) f w_I + bottom pressure torque (corresponding to 9(b)); (b) the streamfunction driven by the bottom pressure torque (corresponding to 10(a)) (c) the streamfunction driven by - f w_I (corresponding to 10(b)). The contour interval is 10 Sv in all plots.

Figure 11c

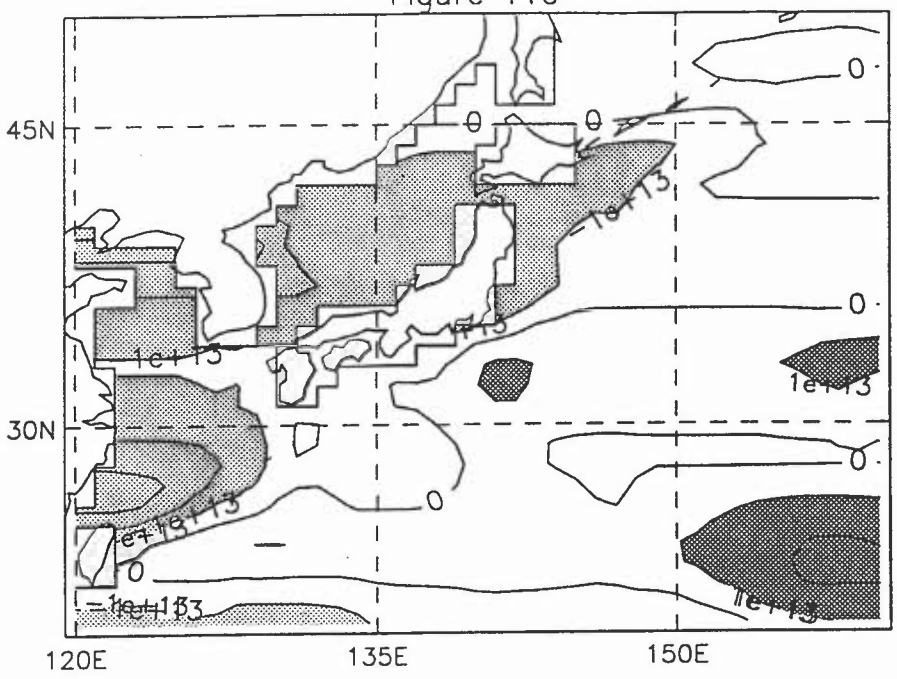

other aspect of the model.

This study has shown that the viscous torque plays an extremely important role in shaping the barotropic circulation of low resolution integrations of the Cox model. As the level of viscous dissipation is determined by numerical requirements rather than physical considerations or field experiments this is unsatisfactory. The level of dissipation can be reduced by increasing the resolution or possibly by using more scale selective forms of dissipation. It may well be, however, that the roughness of the topographic steps and the lego-like nature of the land-sea boundary in the horizontal will keep the viscous drag at high levels close to the topographic steps until the model resolution is significantly improved or the boundary made slippery (Adcroft & Marshall 1997). This could give models which have a smoother coastline (e.g. Myers et al. 1996, Ezer & Mellor 1992) a significant advantage.

5. Concluding Discussion

The main contributions to the tendency of the vorticity of the vertical mean flow and of the vertical integrally integrated flow in the North Atlantic from a short integration of a 1° resolution Bryan-Cox model have been identified (section 3) and compared with the results of GFGL. JEBAR balances the barotropic flow across f/H contours closely whilst the bottom pressure torque and viscous torque are similar in magnitude and together largely balance the local Sverdrup transport. Away from topography the Bryan-Cox code has a good analogue of vortex stretching.

Formulae for the bottom pressure torque (18) and its relationship to the interior bottom vertical velocity (19) have been derived and discussed. At least in the limit of high resolution and low viscous dissipation these formulae indicate that the Cox model should handle the barotropic vorticity well. The contributions to the barotropic streamfunction "forced" by vortex stretching by the interior bottom vertical velocity and by the bottom pressure torque are quite different in the regions of Cape Hatteras and the northern recirculation gyre of the Gulf Stream. The vortex stretching drives a northern recirculation gyre and separation of the Gulf Stream at Cape Hatteras. This result provides a link between the findings of GFGL and integrations of low resolution Cox models. It also suggests an interpretation of the way in which the barotropic circulation is driven (section 5).

The relationship between the bottom pressure torque and bottom vertical velocity is likely to be particularly sensitive to the formulation of the model. In sigma coordinate models (e.g. Blumberg & Mellor 1987) the vertical velocity at the bottom of the model is not forced to be zero (as it is in the Cox model) and the analogue of the curl of the pressure gradient should be calculated entirely at sea points and be identically zero. Similar advantages may be inherent in the isopycnal coordinate model of Bleck & Chassignet (1994). It would be interesting to examine the analogues of (19) in these models and also in the shaved cell formulation of Adcroft et al. (1996) and the layer model of Hurlburt et al. (1996). Intercomparisons between models would be strengthened if they included such diagnostics.

Appendix A Description of FOAM model

The FOAM global model is described in detail by Alves et al. (1995). It uses a uniform 1° grid and has 20 levels, 10 of which are in the upper 300 metres. The topography in the model is based on DBDB5 and has been smoothed using two applications of the 2D form of a 1-2-1 filter. The horizontal viscosity is Laplacian with $\nu = 6000\ m^2s^{-1}$. Horizontal Laplacian diffusion of tracers with $\kappa = 100\ m^2s^{-1}$ is augmented by isopycnal diffusion (Redi 1982) as modified by Gerdes et al. (1991) with $\kappa = 2000\ m^2s^{-1}$ at the surface, $\kappa = 500\ m^2s^{-1}$ at depth and exponential decay of the difference with a half-depth of 500 m. The original second order advection scheme for momentum and tracers is employed with a one hour time step. The model is forced by the well-known climatologies of Hellerman & Rosenstein (1983) for wind stress and Esbensen & Kushnir (1981) for heat fluxes and relaxed towards the Levitus surface temperature and salinities fields with relaxation coefficients corresponding to 35 $W\ m^{-2}\ K^{-1}$. There is a mixed-layer model of Kraus-Turner type which mixes tracers, and Pacanowski & Philander's (1981) scheme for vertical mixing is also employed with the standard choice of parameters. Fourier filtering is used within 15° of the North pole.

Appendix B Advection of thermal field east of Flemish Cap

The thermal gradient in the FOAM model fields in the upper 50 metres near 43 °W, 47 °N is orientated approximately south-east and is about 8 K over 400 km. GFGL (their figure 1) show

a northward flow between about 42 and 44 °W and 45 to 50 °N of about 20 Sv per 3° of longitude. The FOAM model has a flow of similar strength orientated slightly south of east. The topography is very steep close to the Flemish Cap but is about 4000 m at 43 °W, 47 °N.

The depth mean flow corresponding to 20 Sv per 3° of longitude at 45 °N in 4000 m of water is a little over 2 cm/s. Advection by this flow of a temperature gradient of 8 K over 400 km results in a rate of change of temperature of 4 10^{-7} K s^{-1} . After 75 days of integration this results in a 3 K temperature change. Substituting the barotropic flow obtained by GFGL with that obtained in the FOAM model could thus result in a cooling of the magnitude observed in the FOAM model.

6. References

Adcroft, A., C. Hill, and J. Marshall 1996 Representation of topography by shaved cells in a height coordinate ocean model. Submitted to *Mon. Weath. Rev.*.

Adcroft, A., D. Marshall 1997 How slippery are piecewise-constant coastlines in numerical ocean models ? To appear in Tellus.

Alves, J.O.S., Bell M.J., Brooks N.P.J., Cooper A.L., Foreman S.J., Forbes R.M., Sherlock, C.G. 1995 Performance review of the prototype FOAM system. Met. Office Report:FR Tech. Note 159.

Anderson, D. L. T., J. Sheinbaum, and K. Haines 1997 Data assimilation in ocean models. Draft review article.

Beckmann A., Boning C. W., Koberle C., Willebrand, J. 1994 Effects of increased horizontal resolution in a simulation of the North Atlantic ocean. *J. Phys. Oceanogr.*, 24, 326-344.

Bell, M. J. 1997 Momentum fluxes in the Bryan-Cox model. Submitted to *J. Atmos. Oceanogr. Tech.*

Bleck, R., and E. P. Chassignet 1994 Simulating the oceanic circulation with isopycnic coordinate models. In The Oceans: Physical-chemical Dynamics and Human Impact. edited by Majumdar S. K., E. W. Miller, G. S. Forbes, R. E. Smalz and A. A. Panah, pp 17-39, Pennsylvania Academy of Science.

Blumberg, A. F., and G. L. Mellor 1987 A description of a three-dimensional coastal ocean circulation model. In Three-dimensional coastal ocean models, *Coastal Estuarine Sci.*, vol 4, edited by N. Heaps, pp 1-16, AGU, Washington, D. C.

Chao, T., A. Gangopadhyay, F. O. Bryan, and W. R. Holland 1997 Modelling the Gulf Stream system: how far from reality ? *Geophys. Res. Lett.*, in press.

Cox, M. D. 1984 A primitive equation, 3-dimensional model of the ocean. GFDL Ocean Group Tech. Rep. 1, GFDL/NOAA, Princeton, 143 pp.

Dengg, J. A. Beckmann, and R. Gerdes 1996 The Gulf Stream separation problem. The Warmwatersphere of the North Atlantic Ocean Krauss, W. (editor)

Dukowicz, J. K. and R. D. Smith 1994 Implicit free-surface method for the Bryan-Cox-Semtner ocean model. *J. Geophys. Res.*, 99, C4,7991-8014.

Esbensen, S.K. and Kushnir, Y. 1981 The heat budget of the global ocean: an atlas based on estimates from surface marine observations. Climate Research Institute, Oregon State Univ, Corvallis, Report No. 69.

Ezer T., and G. Mellor 1992 A numerical study of the variablity and the separation of the Gulf Stream, induced by surface atmospheric forcing and lateral boundary flows. *J. Phys. Oceanogr.*, 22, 660-682.

Ezer T., and G. Mellor 1994 Diagnostic and prognostic calculations of the North Atlantic circulation and sea level using a sigma coordinate ocean model. *J. Geophys. Res.*, 99, C7, 14159-14171.

Gerdes, R., Koberle C., Willebrand J. 1991 *Climate Dyn.*, 5, 211-226 Role of numerical advection schemes in general circulation models.

Greatbatch, J., Fanning, A. F., Goulding, A. D. and S. Levitus 1991 (GFGL) A diagnosis of interpentadal circulation changes in the North Atlantic. *J. Geophys. Res.*, C12, 96, 22009-22023.

Hellerman, S. and Rosenstein, M. 1983 Normal monthly wind stress over the world ocean with error estimates. *J. Phys. Oceanogr.* 13, 1093-1104.

Hogg, N. G., Pickart, R. S., Hendry, R. M., Smethie, W. J. Jr. 1986 The northern re-circulation gyre of the Gulf Stream. *Deep Sea Res.*, 33, 1139-1165.

Holland, W. R. 1973 Baroclinic and topographic influences on the transport in western boundary currents. *Geophys. Fluid Dyn.*, 4, 336-354.

Holland, W. R. & Hirschman A. 1972 A numerical calculation of the circulation in the North Atlantic ocean. *J. Phys. Oceanogr.*, 2, 336-354.

Hughes C. W. 1995 A warning about topography in the Cox code. *Ocean Modelling*, 106, 8-11.

Hurlburt, H. E., A. J. Wallcraft, W. J. Schmitz Jr., P. J. Hogan, and E. J. Metzger 1996 Dynamics of the Kuroshio/Oyashio current system using eddy-resolving models of the North Pacific Ocean. *J. Geophys. Res.*, 101, C1, 941-976.

Ji, M., Smith, T. M. 1995 Ocean model response to temperature data assimilation and varying surface wind stress: intercomparisons and implications for climate change. *Mon. Weath. Rev.*, 123, 1811-1821.

Killworth P. D., D. Stainforth, D. J. Webb and S. M. Paterson 1991 The development of a free-surface Byran-Cox-Semtner ocean model. *J. Phys. Oceanogr.* 21, 1333-1348.

Levitus, S. 1982: Climatological atlas of the world ocean. NOAA Professional Paper 13.

Mellor, G., Mechoso, C. R., Keto E. 1982 A diagnostic calculation of the general circulation of the Atlantic Ocean. *Deep Sea Res.*, 29, 1171-1192.

Mertz, G., Wright, D. G. 1992 Interpretations of the JEBAR term. *J. Phys. Oceanogr.*, 22, 301-305.

Myers, P. G., A. F. Fanning, and A. J. Weaver 1996 JEBAR, bottom pressure torque and Gulf Stream separation. *J. Phys. Oceanogr.*, 26, 671-683.

Pacanowski & Philander 1981 Parametrisation of vertical mixing in numerical models of tropical oceans. *J. Phys. Oceanogr.*, 11, 1443-1451.

Redi, M. H. 1982 Oceanic isopycnal mixing by coordinate rotation. *J. Phys. Oceanogr.*, 12, 1154-1158.

Richardson, P. L. 1985 Average velocity and transport of the Gulf Stream near 55 °W. *J. Mar. Res.*, 43, 83-111.

Rosati, A., R. Gudgel, and K. Miyakoda 1995 Decadal analysis produced from an ocean data assimilation system. *Mon. Weath. Rev.*, 123, 2206-2228.

Sarkisyan, A.S., and Ivanov, V.F. 1971 Joint effect of baroclinicity and bottom relief as an important factor in the dynamics of sea currents. *Izc. Acad. Sci. USSR Atmos. Oceanic Phys.* Engl Transl., 7, 173-188.

Sarmiento, J. L., and K. Bryan 1982 An ocean transport model for the North Atlantic. *J. Geophys. Res.*, 87, C1, 394-408.

Webb, D. J. 1995 The vertical advection of momentum in Bryan-Cox-Semtner ocean general circulation models. *J. Phys. Oceanogr.*, 25, 3186 - 3194.

Wells, N. C., and B. A. de Cuevas 1995 Depth integrated vorticity budget of the southern ocean from a general circulation model. *J. Phys. Oceanogr.*, 25,2569-2582.